PETROCHEMISTRY OF A LAYERED ARCHEAN MAGMA CHAMBER AND ITS RELATION TO MODELS OF BASALT EVOLUTION

by

Benoit Rivard

Department of Geological Sciences
McGill University, Montréal
December 1985

A thesis submitted to the Faculty of Graduate Studies and Research in partial fulfillment of the requirements for the degree of Master of Sciences.

ABSTRACT

The stratigraphy of Archean greenstone belts is commonly characterized by lower volcanic successions of tholeiitic affinity which are replaced upsection by volcanics ofcalc-alkaline affinity. There is little consensus on the origin of this transition, but in the Abitibi belt Jolly (1975) has suggested that it was produced via crystal fractionation in the many shallow level layered intrusive bodies. In the western Lac Yasinski segment of the La Grande greenstone belt such an intrusion is exposed with its associated system of gabbro feeder dykes and overlying extrusive equivalents. The intrusion is comprised of a core of olivine cumulate with chromite banding and its borders are lined by earlier emplaced coarse-grained gabbros. The overlying volcanic succession is dominated by aphyric basalts to basaltic andesites subdivided into three groups : a lower unit characterized by intermediate Ti values relative to a middle unit of more primitive basalts low in Fe and Ti, and an upper unit displaying very high Ti values. The fine-grained gabbros of the intrusion and the majority of the associated dykes follow an Fe-enrichment trend. Dykes which show field evidence for the assimilation of tonalitic basement, however, follow a trend of Fe-depletion. The Fe-enrichment trend of the uncontaminated gabbros can be modelled by the fractional crystallization of plagioclase, clinopyroxene, and olivine (48:32:20). This model, however, can not account for both the spread in Si and the lack of Fe-enrichment observed in the lavas. Their chemical variations

are best reconciled by a polybaric fractionation model involving komatiitic parental magmas. The apparent Fe-depletion of the basalts and their stratigraphy can be understood in terms of decreasing extents of high pressure fractionation of their parental magma with time which determined the low pressure fractionating assemblage of the magma. Early magmas experienced prolonged residence in subcrustal reservoirs where they fractionated olivine and orthopyroxene. Their residual liquids were saturated in plagioclase and pyroxene at low pressures and underwent gabbroic fractionation before erupting as the early intermediate-Ti lavas. The coarse-grained gabbros of the intrusion appear to represent the cumulate of this process. The later low-Ti lavas are derived from magmas which experienced lesser extents of high pressure fractionation, but underwent excess olivine fractionation at low pressure which produced the olivine cumulates of the intrusion.

When plotted in an AFM projection the basalts and uncontaminated gabbros of the Lac Yasinski segment of the La Grande greenstone belt fall in the field of tholeiitic rocks while the contaminated gabbros fall in the calc-alkaline field. These different trends have developed from a common parental magma in a common tectonic setting. This work suggests that tectonic interpretations of Archean volcanics which rely simply on AFM projections may neglect important aspects of basalt petrogenesis and should be viewed with caution.

SOMMAIRE

La stratigraphie des ceintures de roches vertes archéenes se compose souvent de succession de roches volcaniques tholéiitiques à la base, ensuite remplacées par des roches volcaniques calc-alcalines. Pour de nombreuses intrusions stratifiées de la ceinture de l'Abitibi, Jolly (1975) a proposé une origine par cristallisation fractionnée; l'origine de cette transition demeure toutefois incertaine. Des roches extrusives et un système de dykes de gabbro sont associés à une telle intrusion dans le segment ouest du Lac Yasinski de la ceinture de roches vertes de La Grande. Des cumulats d'olivine et des bandes de chromite se trouvent au centre de l'intrusion alors que des gabbros à grains grossiers antérieurs sont situés en périphérie. Les roches volcaniques se composent principalement de basaltes et d'andésites basaltiques aphyriques et se subdivisent en trois unités: l'unité de base à une teneur intermédiaire en Ti, l'unité centrale se compose de basaltes moins évolués, et pauvres en Fe et Ti, alors que de fortes teneurs en Ti caractérisent l'unitésupérieure. Un enrichissement en fer caractérise la majorité des dykes et les gabbros à grains fins de l'intrusif. Certains dykes démontrent des évidences d'assimilation du socle tonalitique, définissant une lignée d'appauvrissement en fer. L'enrichissement en fer définit par les gabbros non-contaminés peut être reproduit par la cristallisation fractionnée d'un assemblage composé de plagioclase, clinopyroxène et d'olivine (48:32:20). Ce modèle ne peut toutefois reproduire la variation en Si des

laves et l'absence d'enrichissement en fer qui les caractérisent. Un modèle de fractionnation à pression variable impliquant un liquide parental de composition komatiitique peut toutefois expliquer ces variations de composition. Une diminution progressive du degré de fractionnation à haute pression explique la stratigraphie et la lignée d'appauvrissement en fer des basaltes. La nature de l'assemblage de phases fractionnées à basse pression fût defini par ce degré de fractionnation. Les premiers magmas auraient donc fractionné de l'olivine et de l'orthopyroxene causé par une résidence prolongée a l'intérieur de réservoirs situés sous la croûte. A basse pression, les liquides résiduels ont ensuite fractionné plagioclase et pyroxene avant d'être mis en place sous forme de laves à teneur intermédiaire en Ti. Les gabbros à grains grossiers de l'intrusion semblent etre les cumulats resultant de ce procédé. Les laves tardives à basse teneur en Ti ont été dérivées de magmas ayant subi un plus faible degré de fractionnation à haute pression. Par contre celles-ci ont fractionné un excès d'olivine à basse pression et produit les cumulats d'olivine de l'intrusion.

Les basaltes et les gabbros non-contaminés du segment Lac Yasinski se situent dans le champ tholéiitique du diagramme AFM alors que les gabbros contaminés se situent dans le champ calc-alcalin. Ces différentes lignées se sont développées à partir du même liquide parental et du meme environnement tectonique. Cette étude suggère que les

interprétations tectoniques de roches volcaniques archéennes qui ne sont basées que sur des projections AFM peuvent négliger d'importants aspects de la pétrogénèse des basaltes et devraient donc être traitées avec circonspection.

ACKNOWLEDGEMENTS

I wish to express my gratitude to all of those whom in a direct or indirect way have contributed to the completion of this thesis. My greatest appreciation goes to my friend and supervisor, Dr. Don Francis for his guidance and instruction on research methodology; his assistance was available at any time which is something few students can rely on. I also acknowledge the patience and calm he expressed in times where my emotional problems spilled into my academic life. Comments from Dr. B. F. Martin were appreciated in improving parts of this manuscript. Enthusiastic and quick assistance in analytical work was obtained from T. Ahmedali.

Financial support was provided by the Ministère de l'Energie et Ressources (Québec), les fonds F.C.A.C, Max Bell Foundation and Carl Reinhardt Summer Awards. Field work was supported through the Centre for Northern Studies (McGill University), le Ministère de l'Education du Québec, N.S.E.R.C. and Energie Mines and Ressources Canada.

Many ideas arose from late evening discussions in the company of Don Francis, Tom Skulski, Mian Liu, Serge Nadeau and John Todoeschuck and I am greateful to all of them. My friends Richard Forest, Robert Wares and André Lalonde provided unlimited moral support in my bitter moments. Special thanks go to Thor James Brenan who accompanied me for two straight summers in the not so friendly bush of the

James Bay. His good humour and honesty made these four months unforgettable. My final acknowledgement goes to my parents for their constant care and to Jeanne and Robert for their last minute help.

TABLE OF CONTENTS

LIST OF FIGURES

LIST OF TABLES

Page

1 INTRODUCTION

1.1 Archean greenstone belts

Archean greenstone belts are among the oldest crustal material preserved, and retain a record of mafic volcanism on the earth prior to 2.5 b.y. Greenstone belts therefore offer an insight to the magmatic processes operating in the Archean and provide the basic information required to unravel the early volcanic history of the Earth.

Archean greenstone belts are typically deformed geosynclines whose stratigraphic successions are dominated by meta-volcanic rocks and associated hypabyssal intrusive rocks. Many Archean greenstone belts contain tholeiitic, calc-alkaline, and alkaline volcanic suites (Goodwin 1977) and some preserve komatiitic and high-magnesian lavas (Condie 1981, Viljoen and Viljoen 1969). Typically the lower part of the volcanic succession is comprised of ultramafic to mafic tholeiitic volcanic rocks which give way with stratigraphic height to volcanic rocks of calc-alkaline affinity. Examples of such tholeiitic to calc-alkaline successions have been documented in Archean terrains of North America, South Africa and Australia (Viljoen and Viljoen 1970, Jolly 1975, Bickle et al 1983, Gélinas 1984). For example, in the Abitibi greenstone belt, located in the southeastern part of the Superior Province of the Canadian shield, geochemical studies by Jolly (1977) have documented a volcanic stratigraphy whose lower portion is dominated by

primitive tholeiitic basalts with local komatiites. These are overlain by more evolved iron-rich tholeiitic lavas at intermediate levels which in turn are succeeded by iron-poor lavas. Jolly (1980) has documented a complete spectrum of chemical trends in the lavas and has shown that iron-enrichment ('tholeiitic') evolutionary trends are replaced up section by iron-depletion ('calcalkaline') evolutionary trends (Fig. 1). The origin of these two trends and their genetic relationship remains a fundamental problem of igneous petrology. The orderly stratigraphic succession of the two trends, however (Baragar 1966, 1968 Jolly 1977, Goodwin 1977, Taylor and Hallberg 1977) strongly suggests that the later calc-alkalic magmas are genetically related to the earlier tholeiitic magmas. Three mechanisms are commonly proposed to explain the relationship between tholeiitic and calc-alkaline lavas. In the first, the two trends are thought to reflect the differentiation of a common parental magma under different conditions of oxygen fugacity, crustal contamination (Kuno 1950, 1968), or depth at which crystal fractionation occurred (Jolly 1975, Hawkesworth and O'Nions 1977, Jolly 1977, and White and McBirney 1979). In such models, the thickening of the volcanic pile with time is associated with dehydration and eventual melting of the lower crust. The products of these reactions contaminate magmas rising from the mantle and induce the crystallization of phases of low Si content and high FeO/MgO ratio such as amphibole or magnetite. The fractionation of such phases

Fig.1: MgO versus FeO (in weight %) Composite diagram of published compositional trends of lavas from the Abitibi belt. The trends are numbered according to their approximate position in the lava pile. Numbers increase upwards in the stratigraphy. Taken from Jolly (1980).

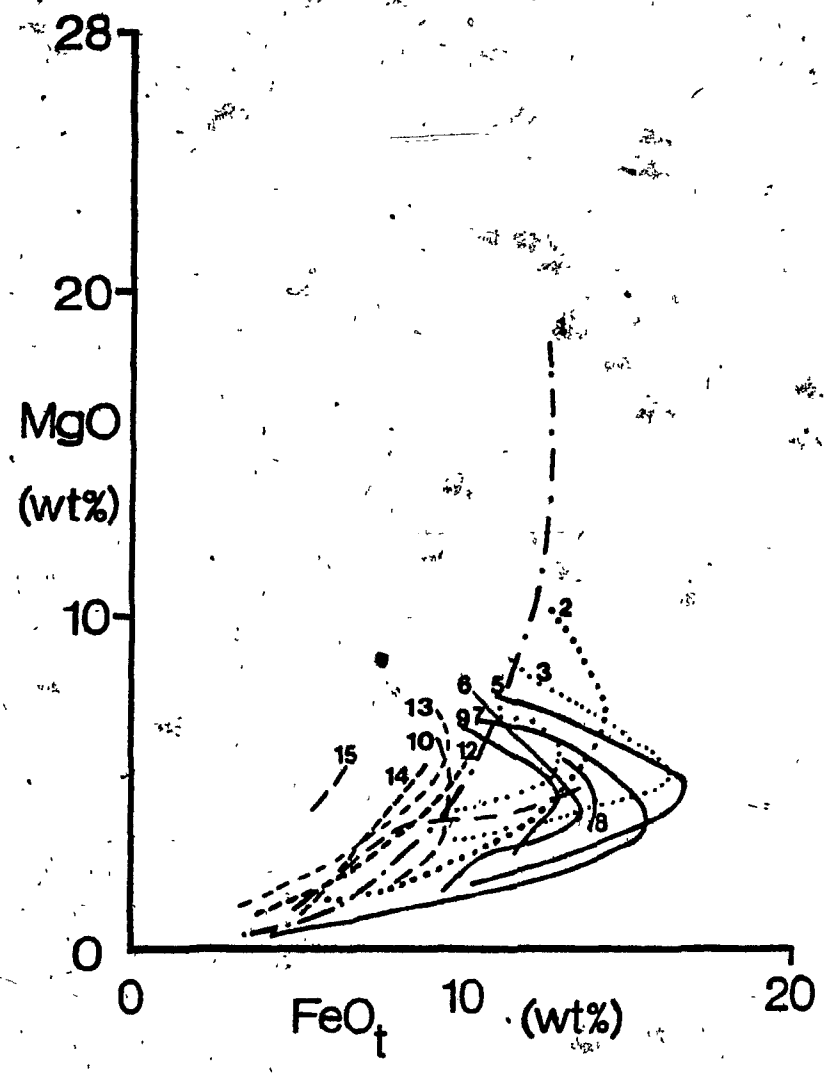

leads to the development of calc-alkaline lavas (O'Nions and Pankhurst 1978). The second explanation is based on a modern plate tectonic analogy and assumes that the early tholeiitic magmas are generated by hydrous melting of mantle above a subducting lithospheric slab undergoing dehydration. At deeper levels partial melts of the subducting slab form acidic magmas which ascend, and hybridize the overlying mantle, providing the source regions for later calc-alkaline magmas (Ringwood 1977). Thirdly some Archean calc-alkaline trends are thought to be produced by increasingly smaller degrees of melting of a source containing residual garnet and/or amphibole (Condie 1976, Davis and Condie 1977, Jahn et al. 1979). All these mechanisms appear to be capable of explaining the temporal change from tholeiitic to calc-alkaline magmas generally observed in Archean greenstone belts. There is at present, however, little consensus because of a lack of physical and chemical constraints on the problem.

The complex structural and metamorphic history which Archean lavas have experienced complicates the recognition of the dominant magmatic process(es) which controlled their chemical evolution. The deformation is often characterized by steeply inclined folds and faults which produce abrupt changes in the lithologies and the loss of stratigraphic components which limit precise lateral correlations. Primary mineralogy is rarely available and petrographic studies often yield inconclusive results. These problems are compounded by

the fact that lavas typically can not be related to equivalent intrusive rocks. The identification of the dominant process(es) which control the enrichment or depletion in iron in lavas is commonly based on the ability of numerical models of such processes to reproduce the observed major and trace element variations. In the Abitibi belt, Jolly (1977) has suggested that the magmas which generated the most primitive lavas could have fractionated at low pressures to produce the overlying basalts of more evolved compositions. According to his model, tholeiitic magmas fractionated olivine and plagioclase to produce Fe-enrichment in the early lavas. The later Fe-depleted lavas were produced by the fractionation of clinopyroxene and magnetite caused by an increase in volatile content of the magma. The rise in volatile content was attributed to deep level fractionation of the source magmas or incorporation of hydrated crustal material. Differentiation in Fred's flow, located in Munro township, Ontario, (Arndt, 1977) may represent an example of magmas related by fractional crystalization. It is a komatiite flow with an initial MgO content approximating 20 wt% which differentiated to a quartz gabbro with 7.5 wt% MgO. The major element composition of the gabbroic differentiate in Fred's flow is indistinguishable from many of the basaltic lavas found in Munro township. The compositional similarity between these rocks provides strong evidence for the involvement of low-pressure fractional crystallization in the genesis of many of

the basalts in this area of the Abitibi belt (Arndt et al. 1977). Jolly (1977) postulated that the many layered intrusive bodies observed throughout the belt represent the high level magma chambers in which this process occurred. This study emphasizes the importance of both intrusive and extrusive rocks to any understanding of magma petrogenesis in the Archean.

1.2 Purpose of the study

This thesis has been part of a larger project undertaken by professors Andrew Hynes and Don Francis to investigate the stratigraphy, structure and petrochemical evolution of the La Grande greenstone belt. It draws heavily on results obtained in previous thesis studies of this project by St-Seymour (1982), Skulski (1985), and Liu (1985) in the La Grande-3 (LG-3) and Lac Guyer segments of the La Grande greenstone belt. My contribution to this project was the investigation of a gabbro-peridotite intrusion and its possible extrusive equivalents in the western segment of the Archean La Grande greenstone belt of northern Québec. In this region, the juxtaposition of a dyke feeder system, a magma chamber, and an overlying volcanic succession offers a unique opportunity to study the processes controlling basaltic magmatism in the La Grande greenstone belt. The documentation of these magmatic processes may improve our understanding of the nature of Fe-enrichment and Fe-depletion trends in Archean volcanics and provide constraints for the origin the temporal evolution of magmatism from tholeiitic

to 'calc-alkaline' which is observed in greenstone belts in general. In this study I am responsible for:

1) the detailed field and petrographic investigation of the Lac Yasinski intrusive complex.

2) the mapping and sampling of the Lac Yasinski basalt stratigraphy along the LG-3 road.

3) the obtainment and interpretation of 153 major element and 66 trace element analyses of the rocks of the intrusive complex and its associated lavas.

The text of this thesis is comprised of two manuscripts for publication which are united with a common abstract and introductory and concluding chapters. The first manuscript appeared as a publication in a symposium volume of the Canadian Institute for Mining and Metallurgy entitled Chibougamau-Stratigraphy and Mineralization (CIM Spec Vol 34, 1984). The second manuscript is to be submitted for publication in Contributions to Mineralogy and Petrology.

2 REGIONAL SETTING OF THE LA GRANDE GREENSTONE BELT

2.1 Location

The La Grande greenstone belt is located north of the Abitibi belt in the James Bay Territory of Québec, at 53° 30'N, 73° 50' - 78° 00'W (Fig. 6). It consists of three discontinuous segments running approximately east-west along the La Grande River reservoir system for an estimated length of 350 km; the eastern Lac Guyer - LG-4 segment, the central LG-3 segment and the western Lac Yasinski segment. The rocks of this region form part of the Superior Province of the Precambrian Canadian shield and have all undergone deformation and metamorphism during the Kenoran Orogeny around 2.5 b.y.

2.2 Previous work and regional geology

The earliest work in the belt consisted of reconnaissance mapping by the Geological Survey of Canada (Eade 1966). In 1974, Mills completed a Ph.D thesis study which included field investigations of the Sakami Lake, Coutaceau Lake and Janjandashi Lake areas. Further regional mapping of the belt was completed by Sharma (1977) and Ciesielski (1984) and a series of more recent detailed maps was produced at a scale of 1/20,000 by the SES group (Fouques et al. 1979), a consortium of Séru Nucléaire, Eldorado Nucléaire and the Société de Développement de la Baie James (SDBJ).

Fouques et al. (1979) divided the stratigraphy of the La Grande area into eleven units as shown in Table 1. The Roches Vertes unit (R.V.) comprises the greenstone succession and was divided into two cycles. The first cycle consists predominantly of ultramafic and mafic lavas, mafic volcaniclastics and iron formations. The second cycle groups intermediate to acidic flows, pillow lavas and conglomerates. Fouques et al. suggest that a discordance separates these two cycles. The basement gneisses are refered to as the 'vieux gneiss' and are isolated from a younger series of gneisses (Serie Laguiche) to the south by a major fault running 070° which is visible on satellite photos. The relationships between the vieux gneiss and the base of the greenstone succession are contradictory. The presence of granitic xenoliths in the LG-3 second cycle volcanics (Skulski 1985), however, suggests that the greenstone succession was erupted on a crust of granitoid composition. In the area of this study the presence of conglomerates which contain angular clasts of tonalitic composition at the base of the supracrustal succession suggests an unconformable relationship between the greenstone and the vieux gneiss. In the Lac Guyer and LG-3 segments however, the vieux gneisses appear to intrude the volcano-sedimentary succession and mask the basement-greenstone contact. These relationships suggest that the granitoid basement must have been locally remobilized either during or after the mafic volcanism of the supracrustal succession.

Table 1. Stratigraphic column of the La Grande area (after Fouques et al. 1979).

PROTEROZOIC	Gabbroic dykes with a diabase texture
	Sakami formation
LOWER APHEBIAN or ARCHEAN	**SERIE LAGUICHE**
	Granites Leucocratic granites, pegmatites Migmatites Biotite-amphibole gneiss
	----------Discordance----------
ARCHEAN	Volcano-sedimentaire (V.S.)
	Arkoses, quartzites, conglomerates, mafic and felsic volcanics, amphibole gneiss, biotite and amphibole schists
	----------Discordance(?)----------
	ROCHES VERTES (R.V.)
	Second cycle:Intermediate to acidic flows, pillow lavas
	----------Discordance(?)----------
	ROCHES VERTES (R.V.)
	First cycle:Iron formations, mafic tuffs, ultramafic and mafic lavas
	----------Discordance----------
	VIEUX GNEISS
	Foliated granodiorite, granites Migmatite-gneiss, orthogneiss

Recent detailed investigations of the supracrustal succession of the La Grande belt include a Ph.D. study by St.Seymour (1982) and M.Sc. study by Liu (1985) in the eastern Lac Guyer segment, and an M.Sc. study by Skulski (1984, 1985) in the central LG-3 segment in an area neighbouring the town of La Grande-3. St-Seymour (1983) has proposed a stratigraphy for the eastern segment of the belt in the vicinity of Lac Guyer which begins with acidic flows, pyroclastics and sediments with intercalated basalts. The Mg# (Mg/Mg+Fe) and abundance of these basalts increases with stratigraphic height towards an overlying succession of komatiitic lavas. The komatiite succession is comprised of a sequence of pillowed pyroxenetic komatiite flows which separates two sequences of peridotitic komatiites. The uppermost unit in the Lac Guyer area consists of a second succession of basalt which are chemically indistinguishable from the basalts at the base of the stratigraphy. Liu (1985) has established a stratigraphy in the volcano-sedimentary succession southeast of Lac Guyer. He has reported the occurrence of two sequences of basalts. The lower basaltic sequence is composed of thick mafic flows interbedded with mafic and felsic tuffs. These are overlain by a second cycle of lavas dominated by pillowed basalts. The basalts in general are characterized by a pronounced Fe-enrichment trend. Pillowed and massive komatiites are observed at the upper stragraphic levels. In the LG-3 segment of the La Grande belt, the lowest levels of the stratigraphy consist

predominantly of a sequence of volcaniclastics and metasediments overlain by a thick succession of submarine basalts with low Mg# and minor basaltic andesites (Skulski et al., 1984). These rocks are overlain by coarse clastics which are in turn overlain by a sequence of basaltic andesites whose evolution is characterized by an iron depletion trend and lower absolute Ti and Fe contents compared to the basalts of the underlying succession. The presence of Fe-enrichment in the lower levels of the volcanic stratigraphy southeast of Lac Guyer and of Fe-depletion in the uppermost LG-3 stratigraphy suggests a temporal evolution of magmatism from tholeiitic to calc-alkaline in the La Grande belt. The basalts of Lac Guyer and of the lowermost LG-3 stratigraphy are characterized by an absence in Fe-trends and may represent an intermediate stage between Fe-enrichment and Fe-depletion trends.

Three phases of deformation are recognized throughout the La Grande belt. The first phase of deformation is penetrative on a centimeter scale and produced the observed schistosity and intrafolial isoclinal folds. The second phase of deformation produced isoclinal folds on a regional scale and open folds on local scale with an average interlimb angle of 30° to 40° degrees, and a steeply dipping fracture cleavage (S-2) varying in orientation from 070° to 120°. These steeply dipping axial planes were the focus of the brittle deformation and were reactivated during later faulting events. The most extensive fault cutting the study

area (Fig. 7) lies along one such plane and produced a prominent local foliation parallel to S-2. The latest deformation event is characterized by subhorizontal kink-bands.

2.3 The Lac Yasinski segment

The topography of the Lac Yasinski region is characteristic of a heavily glaciated terrane with numerous lakes and swamps. Areas which are underlain by granitic and volcanic rocks have a relatively thin glacial cover compared to areas underlain by volcano-sediments. The lower parts of the volcano-sedimentary succession are occupied predominantly by quartz-rich sediments intercalated with minor iron formations and mafic tuffs. The upper parts of the succession are dominated by pillowed and massive lavas which comprise a lower unit of relatively Fe-rich basalts overlain by a thick succession of Fe-poor basalts. These are in turn overlain by the most Fe-rich basalts of the succession. The intrusion of this study is found in the nose of a major synformal F-2 syncline which plunges steeply in the SW direction (Fig. 6). The two major phases of deformation observed in the Lac Yasinski segment have provided a virtually complete cross-section of the intrusion which is located along the contact between a tonalitic basement and the volcano-sedimentary succession overlying it. The presence of basal conglomerates which contain angular fragments of tonalite suggest this contact is an unconformity. Numerous gabbroic dykes cut the basement

tonalites and appear to have fed the intrusion which itself cuts into the basal part of the greenstone succession. The intrusion is thus younger then both the basement tonalites and the lower levels of the greenstone belt and there appears to have been little or no displacement along the basement greenstone contact following its emplacement. These relationships suggest that the gabbroic dykes cutting the basement, the intrusion, and the lavas of the supracrustal succession constitute a comagmatic system which provides a unique opportunity to study the high level processes controlling mafic volcanism in this portion of the La Grande greenstone belt. The following manuscript compares the chemical patterns of the rocks of the Lac Yasinski intrusion to those of the lavas of the La Grande greenstone belt and discusses the nature of the petrogenetic link between the two.

3 PRELIMINARY MODELS FOR BASALT EVOLUTION IN THE LA GRANDE GREENSTONE BELT

Benoit Rivard and Don Francis

Department of geological sciences
McGill University
3450 University St Montréal, Québec H3A 2A7

3.1 Abstract

A layered Archean magma chamber is exposed at the base of the Yasinski segment of the La Grande greenstone belt. This intrusive complex lies beneath a sequence of mafic volcanics and is underlain by granitoid basement which is crosscut by a swarm of gabbroic dykes. The gabbros of both this complex and the dyke swarm define a pronounced Fe-enrichment trend. The volcanic patterns of the La Grande and Eastmain greenstone belts, however, define a series of iron depletion trends which originate in the iron enrichment trend of the gabbroic intrusives. These patterns suggest that the gabbros produced in the intrusive complex may serve as parental liquids for some of the lava suites of the James Bay greenstone belts.

3.2 Introduction

Archean lavas offer a powerful tool for understanding the earth's early history. Iron enrichment ('tholeiitic') and iron depletion ('calcalkaline') evolutionary trends have been recognized in lava successions in many Archean greenstone belts (Jolly 1975, Gélinas, 1984). The identification of the dominant process(s) which produce such trends is based on the ability of models of such processes to

reproduce the observed major and trace element variations. The recognition of the dominant process controlling the evolution of Archean lavas, however, is often made difficult by the complex structural and metamorphic history that these rocks have undergone. Primary mineralogy is rarely preserved and petrographic studies often yield inconclusive results. These problems are compounded by the fact that lavas typically can not be related to equivalent intrusive rocks.

In this paper we present observations obtained through comparing the chemical patterns of intrusive rocks of the complex with those defined by a reconnaissance survey of the regional geochemistry of Archean lavas of the James Bay Territory. A geochemical model is presented which relates the compositions of the lavas to those of the intrusive rocks observed within the layered chamber and dyke system. Stratigraphic and/or temporal variations in this model provide a means of investigating the historical record of magma evolution in the La Grande greenstone belt. In addition, the model provides a useful lithochemical field tool with which to map lateral stratigraphic variations on a regional scale.

3.3 Setting

The La Grande greenstone belt is located in the James Bay Territory of Québec at 53° 30'N, longitude 73° 50' - 78° 00'W. The area was mapped at a scale of 1/100,000 during the late 70's by the Ministère Energie et Ressource du Québec

(Sharma, 1977). A series of more recent maps was produced at a scale of 1/20,000 by the SES group, a consortium of Séru Nucléaire, Eldorado Nucléaire and the Société de Développement de la Baie James (SDBJ).

The La Grande greenstone belt is discontinuous and consists of a number of isolated segments running east-west along the La Grande reservoir system. The intrusive complex of this study is found in the Lac Yasinski segment of the La Grande belt. Here, two major phases of deformation have provided a virtually complete cross-section of a 4 to 5 km thick volcano-sedimentary succession and the plagiogranite basement which underlies it. The intrusive complex lies along this contact at the nose of a first phase syncline where outcrop exposure exceeds fifty percent.

The nature of the granite-greenstone contact is not well defined because it is obscured by the presence of the intrusive complex. There is, however, no evidence of contact metamorphic effects in tuffaceous units adjacent to the basement suggesting that the contact is not an intrusive one. Thin irregular lenses of metaquartzites are found close to the basement contact and grade upwards into a continuous series of thin mafic tuffaceous beds. Mafic tuffs and pillowed lavas appear to dominate the stratigraphy of this segment of the belt. For a more detailed account of the stratigraphy of the La Grande belt, the reader is referred to a companion paper in this volume (Skulski et al., 1984).

3.4 The intrusive complex

The intrusive complex is interpreted to have had a sill-like shape of approximate dimensions 2.5 km long by 1.5 km thick prior to deformation. It consists mainly of a layered ultramafic cumulate (75%). Gabbro is found along both contacts (25%) and occurs predominantly along the upper boundery. The gabbros exhibit chilled margins against the enclosing greenstones, but no visible decrease in grain size is observed at gabbro-ultramafic contacts. Numerous gabbro dykes crosscut the basement granites immediately beneath the ultramafic cumulate and a few intrude the ultramafic cumulate itself. Those intruding the basement display chilled margins along their contacts. Beneath the cumulate pile, gabbros low in Fe and rich in Mg crosscut earlier high Fe gabbros. This relationship suggests that the gabbros may have become less evolved with time during the magmatic evolution of the complex. Partially resorbed xenoliths of the granitic basement and irregular white felsic bands are observed in many of the gabbro dykes indicating that their magma was actively assimilating crustal material at the time of intrusion.

The ultramafic cumulates are serpentinized peridotites which weather to a light brown color. Chromitite layers are observed throughout the majority of the ultramafic body varying in thickness from 20 cm near the gabbro contact exposed in the south to less than a few millimeters near the basement contact. On average, however, these chromite layers

are six to eight millimeters in thickness and alternate with two to three centimeters bands which are poor in chromite.

The primary mineralogy of the ultramafic unit is almost entirely obliterated and the present mineralogy corresponds to lower greenschist facies metamorphic conditions with temperatures on the order of 400-500° C. Olivine pseudomorphs are visible in hand specimen and vary in size from less than 0.5 mm to 3 mm. These pseudomorphs consist of serpentine and exhibit mesh textures and, on rare occasions, hourglass textures. The pseudomorphs preserve the primary oval to equant shape characteristic of olivine growth at slow cooling rates (Donaldson, 1976). The olivine pseudomorphs occupy 80% of the rock volume leaving little doubt as to the cumulus nature of this unit. Although cumulate layering is often difficult to recognized in the field, grain size layering is well defined in thin section. In the chromite poor bands, magnetite-chromite crystals are present in amounts not exceeding 6 to 8%. The matrix between the olivine pseudomorphs is composed of a mixture of fine-grained tremolite, magnetite and magnesite with minor zoisite, chlorite, brucite and talc. This matrix is divided into patchy areas within which tremolite crystals display a common extinction suggesting the former presence of post-cumulus, pyroxene oikocrysts.

The gabbros display a bimodal mineralogy consisting of 20 to 40% plagioclase and 60 to 80% amphibole. Quartz,

epidote, calcite and pyrite are present in minor amounts. Most plagioclase crystals are sericitized or saussuritized. The amphibole is actinolite in the iron-poor gabbros, but hornblende in the iron-rich gabbros and entirely replaces primary clinopyroxene. The pseudomorphed pyroxene crystals are elongated (1-2mm) and some display a herringbone texture.

3.5 Major element geochemistry

The ultramafic cumulates are rich in MgO and low in FeO (Fig. 2, Table 2) and fall close to the olivine composition line in Mg-Fe space. Deviations below this line reflect the amount of intercumulus material, probably largely pyroxene. The large predominance of cumulus olivine in these rocks suggests that the cation Mg/Mg+Fe ratio of the whole rock will approximate the forsterite content of the original olivine. The range of rock compositions suggest that the cumulate olivine ranged in composition from Fo 84 to Fo 89, assuming total iron to be FeO. Although the cumulate rocks display the high loss on ignition (LOI) values characteristic of serpentinites, the clustering of the data observed in figure 2 suggests that major element mobilization during metamorphism is not a serious problem.

The compositions of the gabbros exhibit a striking Fe-enrichment trend with FeO increasing from 4.5 to 14.5% as MgO drops from 18 to 6.5 cation% (Fig. 2). Unlike the gabbroic data, the Yasinski lavas define a continuous trend of decreasing FeO with decreasing MgO. The least evolved lavas

Table 2. Whole rock analyses[a]

[a] Analytical Technique

The lava samples were all taken at the outer margins of pillows or flow tops. The samples used for analysis were ground in tungsten carbide vessels to avoid Ni and Cr contamination. Major elements were determined by X-ray fluorescence using fused pellets. Loss on ignition was determined independently. All analyses are normalized to 100% volatile-free with total Fe as FeO.

	Lavas				Gabbros				Peridotites		
	8304	8311	8306	8314	8351	8343	8346	8393	8375	8358	8392
SiO2	50.27	50.50	51.54	52.18	50.69	49.61	50.37	49.78	42.72	42.61	42.90
TiO2	1.00	0.94	1.03	0.72	0.35	0.43	0.99	1.45	0.05	0.02	0.09
Al2O3	15.26	15.54	15.66	16.67	16.51	13.64	14.47	14.62	1.56	1.48	3.32
Cr2O3	0.05	0.03	0.05	0.06	0.11	0.06	0.03	0.03	0.90	0.51	1.07
FeO2	11.49	12.24	9.79	8.87	7.70	9.72	12.81	14.42	13.07	11.47	12.96
MgO	7.83	7.38	5.64	4.79	11.25	9.86	8.11	6.40	41.38	43.46	38.02
MnO	0.19	0.22	0.18	0.19	0.15	0.20	0.21	0.26	0.14	0.17	0.16
NiO	0.01	0.01	0.01	0.01	0.02	0.02	0.01	0.01	0.16	0.17	0.19
CaO	11.45	10.08	13.72	14.93	10.06	14.87	9.10	10.25	0.00	0.02	1.28
Na2O	2.23	2.57	2.19	1.42	2.82	1.41	2.66	2.17	0.00	0.08	0.00
K2O	0.14	0.42	0.13	0.12	0.32	0.13	1.17	0.50	0.01	0.00	0.00
P2O5	0.07	0.06	0.06	0.03	0.02	0.04	0.07	0.11	0.01	0.00	0.00

Fig. 2: Cation % Mg - Fe. Gabbroic dyke complex, ultramafic cumulates and Lac Yasinski lavas. Ultramafic cumulate, diamonds; gabbros, triangles; Lac Yasinski lavas, circles. In the bottom figure the field of Lac Yasinski lava compositions is indicated by the dashed line and the liquids capable of coexisting with the cumulate compositions are defined by the dashed arrows. In the top figure the field of gabbro compositions is enclosed by a dashed line.

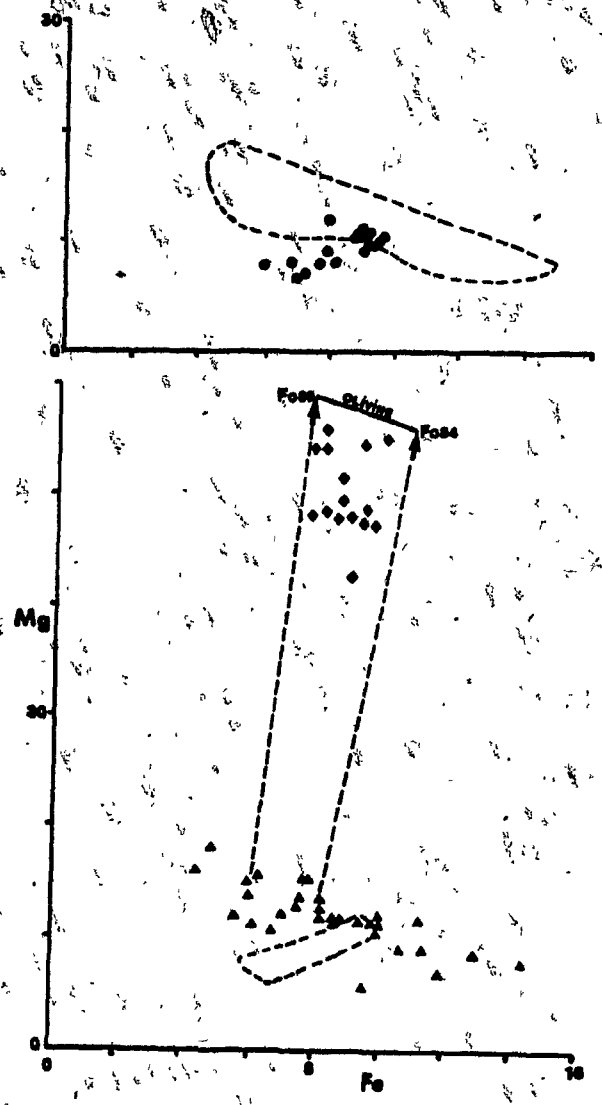

of this suite, however, overlap the field of gabbroic compositions. This overlap between the gabbros and most primitive lavas is also observed for elements such as aluminum, silicon, titanium and chromium. Plots of alkalies and calcium, however, display considerable scatter, suggesting the effects of alteration. For this reason sodium and potassium were excluded during the later modelling of compositional trends.

3.6 Discussion

A genetic relationship between the gabbros and ultramafic rocks was tested assuming a KD of 0.3 for the distribution of Fe and Mg between olivine and liquid (Roeder and Emslie, 1970, Roeder, 1974). This value is generally accepted as being appropriate for most terrestrial basalts. The range of gabbroic liquids capable of coexisting with the observed ultramafic cumulate includes most of the least evolved gabbros (Fig. 2). These gabbros correspond to the largest dykes in the underlying basement and to the gabbros located immediately above the cumulate pile. In the basement, they represent a small portion of the total volume of gabbros present. The volume of gabbro at the top of the intrusion is small in comparaison with the volume of olivine-chromite cumulate. It follows that if the ultramafic and gabbroic rocks were genetically related, then a large amount of gabbroic liquid must have past through this intrusive complex and been removed to account for the paucity of observed gabbro.

The composition of olivine in equilibrium with the least evolved lavas is approximately Fo 80, a value below the minimum value of Fo 85 estimated for the cumulates. If 15% of the total iron in these gabbros is converted to ferric iron, the calculated olivine composition increases to Fo 82, still below that capable of having produced the cumulates.

Fractional crystallization is the most common process called upon to explain the chemical variation in igneous rocks. It was used in attempts to reproduce the trend observed for the gabbros. A model involving more than 50% crystallization of an assemblage composed of 20% olivine, 32% clinopyroxene and 48% plagioclase is required to reproduce the range of observed gabbros (Fig. 3). The effects of assimilation, as evidenced by the presence of basement xenoliths within the gabbros of the dyke complex, will probably reduce the amount of fractionation required to produce the observed variation. The testing of the magnitude of these effects must await the availability of trace element data on these rocks.

The lavas of Lac Yasinski are aphyric so it is impossible to determine the actual liquidus phases. Lavas of similar composition containing plagioclase and pyroxene phenocrysts are found in the LG-3 area (Skulski et al., 1984) and compositionally similar plagioclase glomeroporphyritic basalts are a recurring phenomenon in Quebec greenstone belts. In modelling a fractionation process which could have

Fig. 3: Cation % Mg - Fe. Crystallization paths modeled for the gabbros and lavas. The field of gabbroic compositions is indicated by the dashed line. The field of lava compositions is indicated by the dotted pattern. The calculated fractional crystallization path for gabbros is indicated by arrow 1. Equilibrium crystallization paths for the lavas are indicated by arrow 2 (100% olivine) and arrow 3 (10% olivine 40% cpx, 50% plagioclase). Fractional and equilibrium crystallization were modeled using a finite-difference technique. The fractional crystallization model consisted of the repeated calculation of the instantaneous equilibrium compositions of crystals coexisting with the liquid. Each step involved the removal of a quantity of these phases equivalent to 0.01 cation per cent of the initial parent and the recalculation of the residual liquid to 100 percent. The equilibrium crystallization model involved steps of a constant decrease in the MgO content of the liquid. The amount of residue increased with each step and was allowed to reequilibrate with the liquid such that the bulk composition remained fixed. The olivine composition was computed using Roeder and Emslie's (1970) value of the Fe/Mg KD of 0.3 and was combined to their geothermometer to yield an equilibrium temperature. This temperature value was then used to define the Fe/Mg ratio of the clinopyroxene using the equations of Gamble and Taylor (1980).

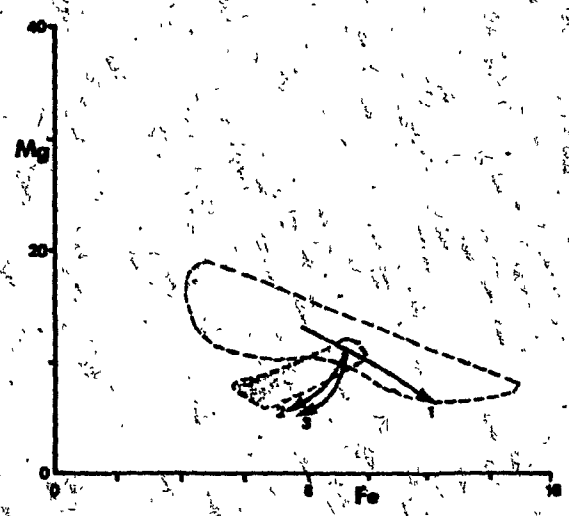

controlled the chemical evolution of the lavas, the most restricting factors are the significant decrease in total iron with only a minimal increase in SiO_2. Fractional crystallization lines for olivine are steep in this region of the MgO-FeO diagram and therefore cannot produce the iron depletion displayed by the lavas (Langmuir and Hansen, 1980). The crystallization of reasonable amounts of chromite and calculation of a portion of Fe as Fe_2O_3 helps, but are still incapable of producing the required Fe depletion. The involvement of pyroxene and plagioclase would all force liquid compositions to higher iron contents. An equilibrium crystallization model involving the extraction of the mineral phases in a single step, produces a better fit with the observed lava compositions (Fig. 3) for an assemblage composed only of olivine whose calculated compositions range from Fo 68 to Fo 77. However, it still fails to produce the degree of Fe depletion observed. A more reasonable assemblage composed of plagioclase, olivine and clinopyroxene (Fig. 3) yields an inferior fit which worsens if the ferric/ferrous iron ratio is raised. What appears to be required is the involvement of an iron oxide phase.

The most Mg rich compositions of the Lac Yasinski lavas lie within the field defined by the gabbros. Reconnaissance geochemical transects across other segments of greenstone belts in the James Bay Territory all exhibit well defined iron depletion trends (Fig. 4) similar to the one observed in the Lac Yasinski lavas. The overall pattern is

Fig. 4: Cation % Mg - Fe. Compositions and trends of lava suites from across the La Grande and Eastmain belt are compared to the field of gabbroic compositions from the Lac Yasinski intrusive. In the top figure the Lac Guyer lava compositions are plotted as open circles and the Eastmain lava compositions as half circles. The Lac Guyer data are from Stamatelopoulou-Seymour et al. (1983). In the bottom figure the Eastmain lava suite corresponds to arrow 1, the Lac Yasinski lava suite to arrow 2 and the Lac Guyer lava suite to arrow 3.

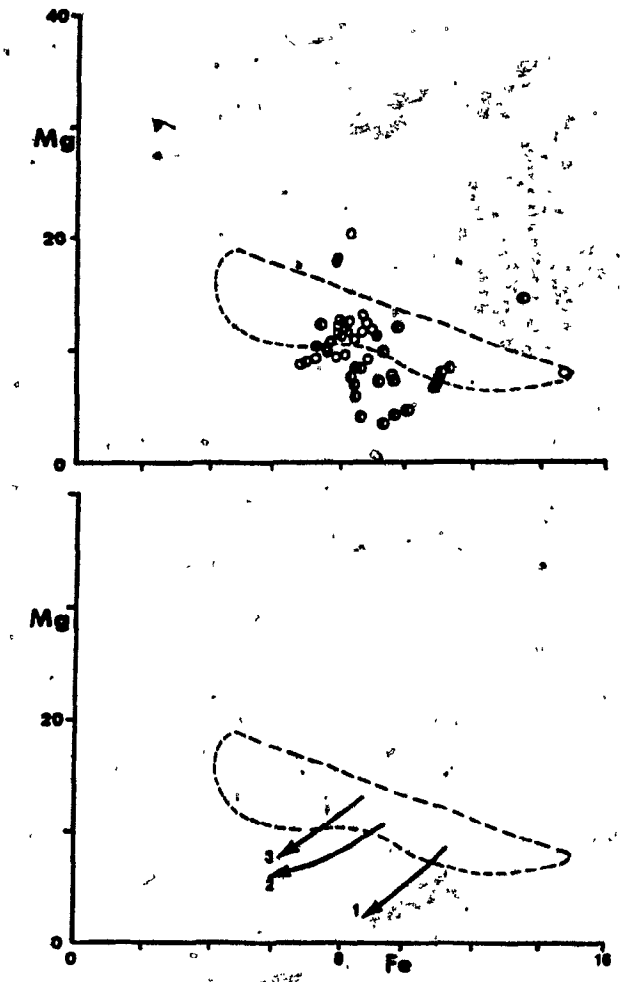

one of a series of subparallel iron depletion trends (Fig. 4), which are slightly offset in Mg-Fe space. Jolly (1975, 1980) has reported a similar overall pattern for the lavas of the Abitibi greenstone belt. In every case the least evolved liquids lie within the field of gabbro composition observed in the Yasinski intrusive complex. These observations suggest that the gabbros produced in the intrusive complex may represent the spectrum of parental liquids for some of the lava suites of the James Bay greenstone belts. The different lava suites may all have been derived from similar parental magmas which embarked on Fe-depletion trends at differing points during their compositional evolution.

3.7 Conclusion

An ultramafic sill of cumulate olivine and chromite is exposed at the base of the Yasinski segment of the La Grande greenstone belt. It is underlain by a system of crosscutting gabbroic dykes and overlain by a suite of mafic lavas. From a crystal fractionation point of view, the lavas and gabbros appear to have evolved along very different liquid lines of descent. The gabbros display an iron enrichment trend typical of tholeiitic suites while the lavas display an iron depletion trend. Fractional crystallization models lead to a satisfactory solution for the gabbros, but can not reproduce the observed lava trends (Fig. 3). The best fit for the latter is obtained by a model involving the equilibrium crystallization of olivine alone or with an opaque followed by a single step batch fractionation of these phases. The

likelihood of the presence of liquidus phases other than olivine cannot be discarded. However, if present, they are apparently not being extracted from the melt. The least evolved lavas, of each of the three lavas suites examined, fall in the gabbroic compositional field (Fig. 4). This suggests a genetic relationship between the lavas suites and the gabbros observed beneath the cumulate pile. The gabbros are thought to have evolved by fractional crystallization during their ascent and emplacement in sill reservoirs at high crustal levels. These magmas then evolved to produce the Fe-depletion trends observed in the lavas compositions. The factor(s) which control the transition from a trend of iron enrichment to one of iron depletion during magma evolution are poorly understood at present. They may involve an increase in oxidation state with the concomittant appearance of an opaque phase on the liquidus (Osborn, 1959). Alternatively, an increase of magma viscosity and density during fractionation may reduce the efficiency with which magmas can rid themselves of crystals. Crystals would remain suspended and be more likely to equilibrate with their host magma before segregation by a process such as filter pressing. We are presently investigating these possibilities by comparing the compositions of lavas suites on different Fe-depletion trends from the James Bay greenstone belts.

4 SUMMARY OF RESULTS AND STATEMENT OF THE GOALS OF THE SECOND PUBLICATION

The preceding publication documented the existence of an apparent correlation between compositions of extrusive rocks of the La Grande and Eastmain greenstone belts and the compositional spectrum of the Lac Yasinski intrusion. The gabbros of the Lac Yasinski intrusion define a compositional trend of increasing Fe with decreasing Mg. The volcanic patterns of the James Bay greenstone belts, however, define a series of iron depletion trends which appear to originate at different positions along the compositional spectrum of the Yasinski gabbros. This suggested that the more primitive lavas which overlap the spectrum of gabbro compositions were the extrusive equivalents to the gabbros of the Lac Yasinski intrusion. The factor(s) which controlled the transition from the iron enrichment trend of the intrusive gabbros to the iron depletion displayed by the lavas, however, was poorly understood. Fractional crystallization models reproduced the chemical variation observed in the gabbros, but were not succesfull in generating the iron depletion trends observed in the lavas. In addition, it was unclear whether the magmas of the lavas had evolved along apparent iron depletion trends (Fig. 5 path a) or whether these trends represented the locus of a series of liquids which had overshot the plagioclase-pyroxene cotectic represented by the spectrum of gabbroic (Fig. 5 path b) compositions.

Fig. 5: Mg versus Fe (in cation %) Schematic representation of possible magma evolution paths leading to the formation of iron depletion trends. See text for explanations.

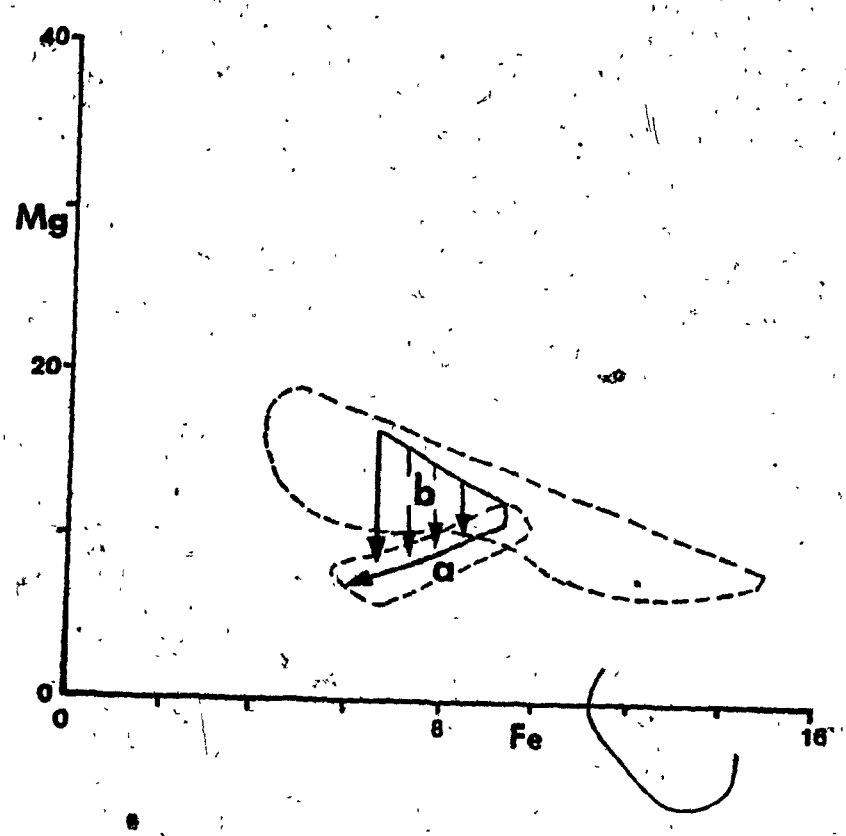

New field observations and analyses of samples acquired during the summer of 1984 indicated the existance of three distinctive lava populations in the volcanic succession of the Lac Yasinski greenstone belt based on the concentrations of Ti and Fe. The earliest lavas contained intermediate values of Ti and Fe and were succeeded upwards by voluminous lavas with more primitive compositions low in Fe and Ti. The fact that these more primitive lavas were richer in Si than their more evolved predecessors suggested a mechanism involving a combination of high and low pressure crystal fractionation which would explain the differences between the compositional spectrum of the gabbros of the Lac Yasinski intrusion and the spectra of lava compositions. The following paper presents this model and examines its implications for the origin of iron enrichment and iron-depletion trends in the magmas in the La Grande greenstone belt.

5 PETROCHEMISTRY OF AN ARCHEAN MAGMA CHAMBER AND ITS RELATION TO MODELS OF BASALT EVOLUTION.

Benoit Rivard and Don Francis
Department of Geological Sciences, McGill University
3450 University St, Montreal, Quebec H3A 2A7

5.1 Abstract

It has been proposed that shallow-level intrusions represent the dominant site of the fractionation history which is recorded in the chemical stratigraphy of Archean lavas. The relict of such a low pressure magma chamber is preserved along the basement-supracrustal contact of the Lac Yasinski segment of the La Grande greenstone belt. The intrusion is associated with a gabbro dyke swarm in the underlying granitoid basement and appears to constitute part of the feeder system to the overlying volcanic succession. Its core is comprised of an olivine cumulate peridotite with chromite banding and its borders are lined by massive coarse-grained gabbros which appear to predate the peridotite. The volcanic succession of the overlying greenstone belt is dominated by massive and pillowed aphyric basalts to basaltic andesites that have been metamorphosed to mid-greenschist facies. These basalts are subdivided into three groups : a lower unit characterized by intermediate Ti values and low Si abundances relative to a voluminous middle unit of more primitive basalts which are low in Fe and Ti, and an upper unit displaying very high Ti values. The fine-grained gabbros of the intrusion and associated dyke swarm follow an Fe-enrichment differentiation trend which can be modelled by the fractional crystallization of plagioclase, clinopyroxene,

and olivine (48:32:20) and lie along a low pressure cotectic which approximates that determined experimentally by Spulber and Rutherford (1983). This model, however, can not account for both the spread in Si and the lack of Fe-enrichment observed in the overlying lavas. The chemical variations of these basalts are best reconciled by a polybaric fractionation model involving komatiitic parental magmas. According to this model, the volcanic stratigraphy of the Lac Yasinski segment reflects decreasing extents of high pressure fractionation of these komatiitic parental magmas with time. In the early stages of volcanism, magmas experienced prolonged residence in subcrustal magma reservoirs where the fractionation of olivine and orthopyroxene produced residual liquids which were saturated in pyroxene and plagioclase at low pressures. These liquids underwent gabbroic fractionation at low pressures before erupting as the early intermediate-Ti lavas. The coarse grained gabbros of the Lac Yasinski intrusion represent the cumulate produced by this fractionation process. The later low-Ti lavas are derived from magmas which experienced lesser extents of high pressure fractionation, but underwent extensive olivine fractionation as they rose to the surface, producing the olivine cumulates which dominate the core of the Lac Yasinski intrusion. The absence of the development of a Fe-enrichment trend in the Yasinski lavas appears to reflect a systematic overshooting of the plagioclase-pyroxene cotectic as defined by the gabbros of the intrusion. The only magmas which evolved

towards Fe-poor compositions are gabbroic dykes which show macroscopic evidence of the assimilation of the tonalitic basement.

5.2 Introduction

Archean greenstone belts preserve detailed records of the Earth's early volcanic history. The existence of both iron-enrichment ('tholeiitic') and iron depletion ('calc-alkaline') differentiation trends in Archean volcanic suites is well documented (Jolly 1975, Sun and Nesbitt 1978, Gélinas 1984) and studies of the geochemistry of the Abitibi greenstone belt demonstrate that there is a continuous spectrum of differentiation trends between these two end-members (Jolly 1977). Jolly has observed that the most strongly Fe-enriched lavas occur near the base of the stratigraphy whereas the volume of Fe-depleted lavas increases up section. He has suggested that the compositional variations of the Abitibi lavas was primarily controlled by crystal fractionation at low pressures in layered intrusive bodies found throughout the belt. An examination of such Archean intrusive complexes may thus provide the means to establish the role of low pressure fractionation processes and enable the recognition of the effects of other processes which may have modified magma compositions prior to their emplacement at shallow levels.

This study presents the results of an investigation of a layered intrusion and its extrusive equivalents in the

western segment of the Archean La Grande greenstone belt of northern Québec. In this region, the juxtaposition of a dyke feeder system, a layered magma chamber, and an overlying volcanic succession offers a unique opportunity to study the processes controlling basaltic magmatism in the La Grande greenstone belt. The documentation of these magmatic processes may improve our understanding of the origin of Fe-enrichment and Fe-depletion trends in Archean volcanics and provide constraints for the origin of the temporal transition from 'tholeitiic' to 'calcalkaline' evolutionary trends which is observed in greenstone belts in general.

5.3 Regional setting

The La Grande greenstone belt is located in the James Bay Territory of Québec at 53° 30'N, between 73° 50' and 78° 00'W (Fig. 6). The area was mapped at a scale of 1/100,000 during the late 1970's by the Ministère d'Energie et des Ressources du Québec (Sharma, 1977). A series of more recent maps was produced at a scale of 1/20,000 by the SES group, a consortium of Séru Nucléaire, Eldorado Nucléaire and the Société de Développement de la Baie James (SDBJ).

The La Grande greenstone belt is discontinuous and consists of three isolated segments running approximately east-west along the La Grande reservoir system; the eastern Lac Guyer-segment, the central LG-3 segment, and the western Lac Yasinski segment. The metamorphic grade shows an overall increase eastwardly along the belt from greenschist facies in

Fig. 6: Regional map of the Lac Yasinski segment of the La Grande greenstone belt

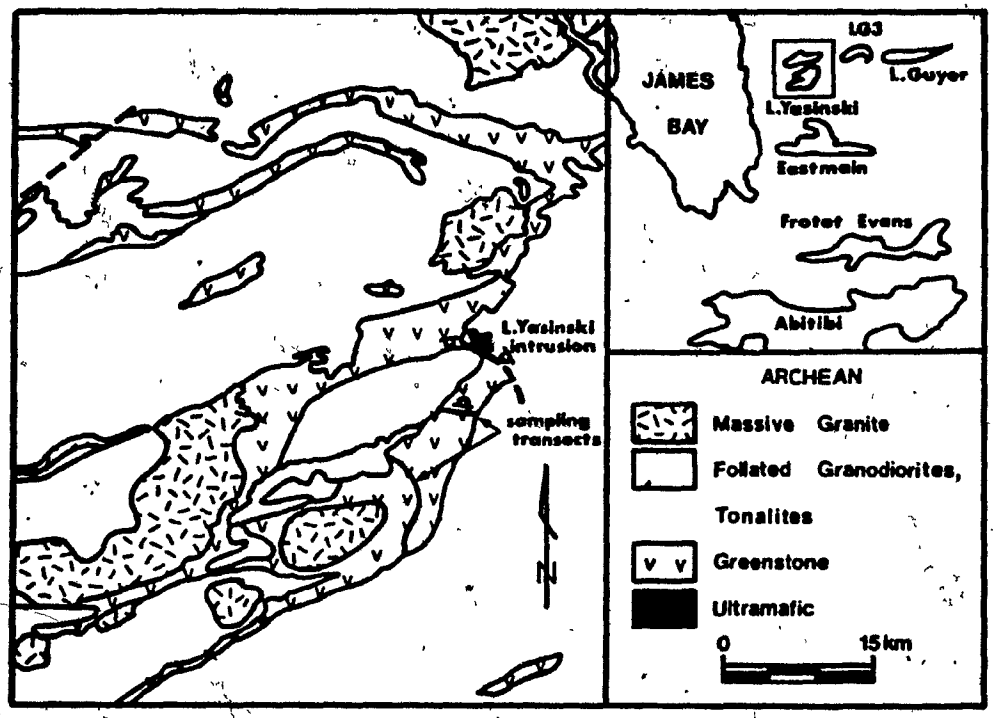

the Lac Yasinski segment to amphibolite facies in the LG-4 area. Previous petrological studies in the belt include work by St.-Seymour (1982), St-Seymour et al. (1983) and Liu (1984) in the eastern Lac Guyer segment and by Skulski et al. (1984) and Skulski (1985) in the central LG-3 segment. In the eastern Lac Guyer segment, the volcanic succession begins with acidic flows, pyroclastics and sediments with intercalated basalts which increase in abundance up section. The Mg# (Mg/Mg+Fe) of the basalts increases with stratigraphic height towards an overlying succession of komatiitic lavas. This succession comprises a sequence of pillowed pyroxenitic komatiite flows which separates two sequences of peridotitic komatiites. The upper-most part of the preserved stratigraphy consists of a second basalt succession which overlies the komatiites. The close spatial relationship of the Lac Guyer basalts and komatiites suggests that they are genetically related and led St-Seymour et al. (1983) to propose that members of the komatiitic suite may have served as parental magmas for the basalts.

In the LG-3 segment of the La Grande belt, the lowest levels of the stratigraphy consist predominantly of a sequence of volcaniclastics and metasediments overlain by a thick succession of submarine basalts with low Mg# and minor basaltic andesites (Skulski et al. 1984). These rocks are overlain by coarse clastics which are in turn overlain by a sequence of basaltic andesites whose evolution is characterized by an iron depletion trend and lower absolute

Ti and Fe contents compared to the basalts of the underlying succession. Skulski (1985) has proposed that these basaltic andesites were the product of the assimilation of a rhyolite contaminant by a komatiitic magma.

In the western Lac Yasinski segment of the La Grande belt, two major phases of deformation have exposed a 4-5 km thick section consisting of a granitoid basement overlain by a volcano-sedimentary succession which is comprised of clastic and volcanoclastic sediments, pyroclastic deposits and pillowed basalts (Fig. 6). In the area of the intrusion, the basement rocks are tonalites characterized by equal proportions of coarse-grained plagioclase and quartz. The base of the volcano-sedimentary sequence is composed of clastic sediments dominated by quartzites and quartz-rich greywackes. Local conglomerates contain angular clasts similar in appearance to the underlying tonalitic basement rocks suggesting an unconformable relationship between the tonalite basement and the greenstone. This conclusion is supported by the absence of xenoliths of greenstone in the tonalites in this area or any sign of a contact metamorphic aureole in the greenstone adjacent to the tonalite. The upper parts of the greenstone belt stratigraphy are dominated by mafic pillowed and massive lavas with associated volcaniclastic-sediments and minor iron formations. Regional metamorphism in this part of the belt falls in the mid-greenschist facies, but grades up to amphibolite facies in the proximity of late granite plutons which intrude the

greenstone.

5.4 The intrusion

The intrusion lies along the basement-greenstone contact in the nose of a second phase syncline at the eastern end of the Lac Yasinski greenstone segment. It is interpreted to have had a shape approximating that of a 1 km thick sill which intruded upwards into the volcano-sedimentary succession (Fig. 7). The contact between the intrusion and the base of the volcano-sedimentary succession is marked by prominant metamorphic effects which include grainsize coarsening of mafic tuffaceous rocks and the development of a blue tint in the quartz of the adjacent clastic sedimentary rocks. These metamorphic features define a 2-30 m wide aureole which is irregularly distributed about the intrusion. Massive gabbros and layered peridotite comprise most of the volume of the complex. The peridotites dominate the core of the intrusion and are completely serpentinized, consisting of an assemblage of serpentine, tremolite, zoisite, chlorite, magnetite, talc and calcite (Fig. 7). Their primary mineralogy has been obliterated, but pseudomorphs (0.5mm-3mm) displaying mesh and rare hourglass textures (Wicks, 1977) preserve the equant and oval shapes of magmatic olivine grains. The olivine pseudomorphs are commonly surrounded by tremolite crystals which display a common extinction and appear to replace poikilitic pyroxene. Layering is defined by the presence of chromite-rich bands (>95% modal chromite) which alternate with horizons rich in

Fig. 7: Detailed map of the Lac Yasinski intrusion

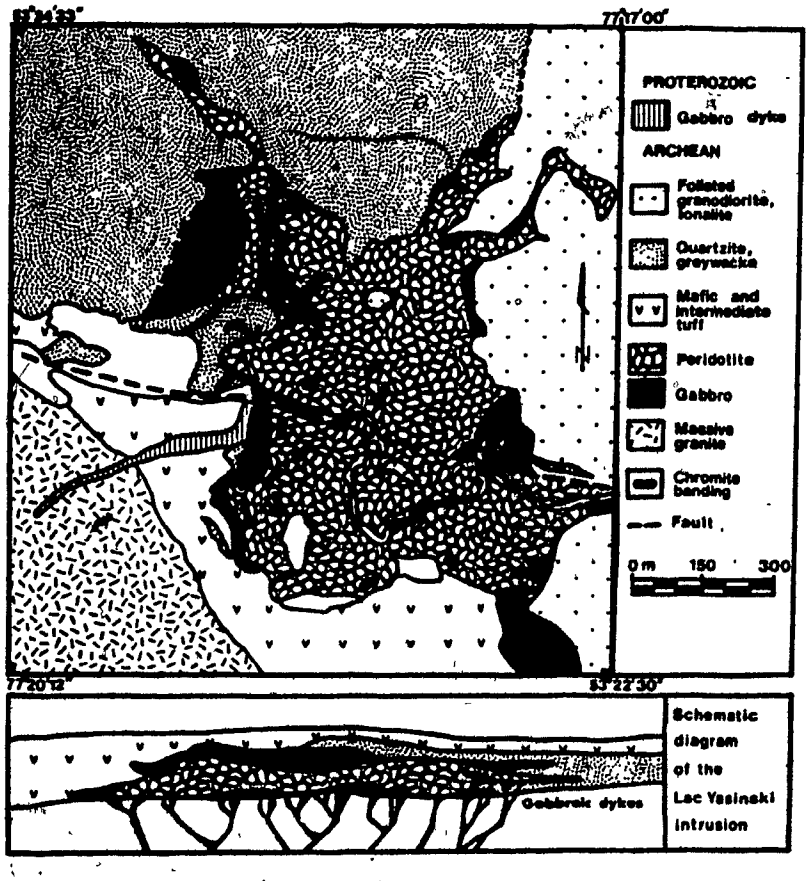

olivine pseudomorphs (<3% modal chromite). These bands are restricted to the upper half of the peridotite pile and display an average thickness of 6 to 8 mm. The thickest chromitite layers (20 cm) are found at the top of the pile near the gabbro-peridotite contact. The large percentage of the rock volume (up to 85 modal %) occupied by the olivine pseudomorphs in addition to the regularity of the chromite banding leaves little doubt that the peridotite represents an olivine-chromite cumulate with post-cumulus clinopyroxene. The present metamorphic mineral assemblage of this ultramafic cumulate pile and the style of folding in the chromitite bands indicates that the intrusion has undergone the same folding and metamorphic history as the overlying volcanics of the greenstone belt (Fig. 7).

Gabbro occurs as lenses along both the top and bottom contacts of the intrusion, but predominates along the roof. No decrease in grain size was observed at the contact between gabbro and peridotite. The gabbros display a bimodal mineralogy consisting of medium- to coarse-grained plagioclase and actinolite in sub-equal proportions (plagioclase:actinolite, 40:60 to 50:50). The subhedral and equigranular nature of plagioclase and actinolite suggest that plagioclase and pyroxene crystallized simultaneously. The coarseness of these gabbros implies that they may have a cumulate origin. Plagioclase is commonly saussuritized and replaced by epidote and calcite with quartz and chlorite present as minor constituents. Exsolution lamellae

symetrically disposed about central twin plane are occasionally observed in actinolite crystals. Such texture suggests the replacement of inverted pigeonite and would imply the former presence of two pyroxenes in the coarse-grain gabbros. The local occurrence of intrusive breccias within the gabbros of the intrusion may indicate that multiple pulses of gabbroic magma were involved in the history of the intrusion.

Numerous gabbro dykes with fine-grained 'chilled' margins crosscut both the tonalitic basement underlying the intrusion and the metasedimentary rocks adjacent to the intrusion. These gabbroic dykes are petrographically similar to the gabbros of the intrusion and the decrease in density and proportion of these dykes away from the main intrusion indicates that the intrusion and the dykes are comagmatic. The fine grained nature of these dyke rocks suggest that they approximate frozen liquids. Larger gabbro dykes (up to 80 m) with high Mg# typically crosscut smaller dykes (= 5 m) with lower Mg# suggesting that the gabbroic magma may have become progressively less evolved and more voluminous with time.

Although a few gabbro dykes intrude the peridotite, none could be traced across the entire intrusion. Such dykes display symmetric borders (0.2 to 1 m) against the peridotites which are rich in acicular tremolite. The amphibole crystals appear to replace clinopyroxene, which

persists locally as relict cores. Domains rich in olivine pseudomorphs (2-5 mm) are also observed locally. This border unit appears to represent a clinopyroxenite produced by reaction between a late gabbroic liquid and the cumulate olivine of the peridotite.

Some dykes cutting the basement contain abundant xenoliths of the host tonalites. Although many of these fragments display sharp contacts with their gabbroic matrix, others appear to have been partially resorbed and are commonly associated with the presence of megacrysts and glomerocrysts of plagioclase. Pegmatitic gabbros which are spatially related to small fragments of tonalite and greywacke in the main intrusion may represent a similar phenomenon. These xenolith-bearing dykes commonly display granophyric intergrowths of feldspar and quartz in their matrix which may reflect the assimilation of felsic material.

5.5 The volcanics

Two transects were measured across the volcanic succession of the Lac Yasinski belt (Fig. 6). The northern transect contains the greatest outcrop exposure and thus offers the most detailed stratigraphy. Its lowest parts are occupied predominantly by quartz-rich sediments intercalated with minor iron formation, mafic tuffs and pillowed basalts. These give way to a continuous succession of pillowed basalts capped by a thin sequence of intercalated pillowed basalts and mafic tuffs. These are in turn overlain by a second

succession of pillowed basalts which is topped by an iron formation and a tuffaceous horizon. A 180 m gap in exposure separates this sequence from an overlying group of pillowed basalts observed at the highest levels of the stratigraphy. Only the chilled margins of pillows were sampled in order to identify phenocryst phases and to minimize the possible effects of compositional variation associated with crystal accumulation, differential alteration or metamorphic recrystallization. The majority of these basalt samples are aphyric with the exception of two which contain glomeroporphyritic plagioclase pseudomorphs. The lavas are dominated by a fine-grained matrix composed of plagioclase and actinolite replacing pyroxene. Plagioclase is in most cases saussuritized and typically minor amounts of chlorite, epidote, apatite and pyrite are present.

5.6 Geochemistry

The peridotites are rich in Mg and extend towards an olivine composition line in Mg-Fe space (Fig. 8a) (Table 3). Because olivine is the main phase in these rocks, the range of Mg# (Mg/Mg + Fe, cation units) of the bulk rocks gives a minimum estimate of cumulus olivine compositions (Fig. 8a), which appear to have ranged between Fo 81 and Fo 88. The spread of the peridotites from the olivine line (Fig. 8a) towards lower Mg values in part reflects the increasing proportion of post-cumulus interstitial pyroxene and the presence of chromite in the peridotites. The clinopyroxenite reaction borders contain lower Mg and Fe but higher Ca and Al

Fig. 8: **a and b** Mg versus Ti and total Fe (cation units) for the Lac Yasinski intrusive rocks. Peridotites, solid triangles; pyroxenites, open triangles; coarse-grained gabbros, solid circles; fine-grained gabbros, open circles; tonalites+ greywackes, open hexagons. **Fig. 8.c and d** Mg versus Ti and total Fe (cation units) for the Lac Yasinski extrusive rocks. High-Ti basalts, solid squares; intermediate-Ti basalts, half-filled squares; low-Ti basalts, open squares; contaminated gabbros, solid stars. The arrow marks the low pressure fractionation path followed by a primitive Morb basalt as determined from melting experiments (Spulber and Rutherford 1983)

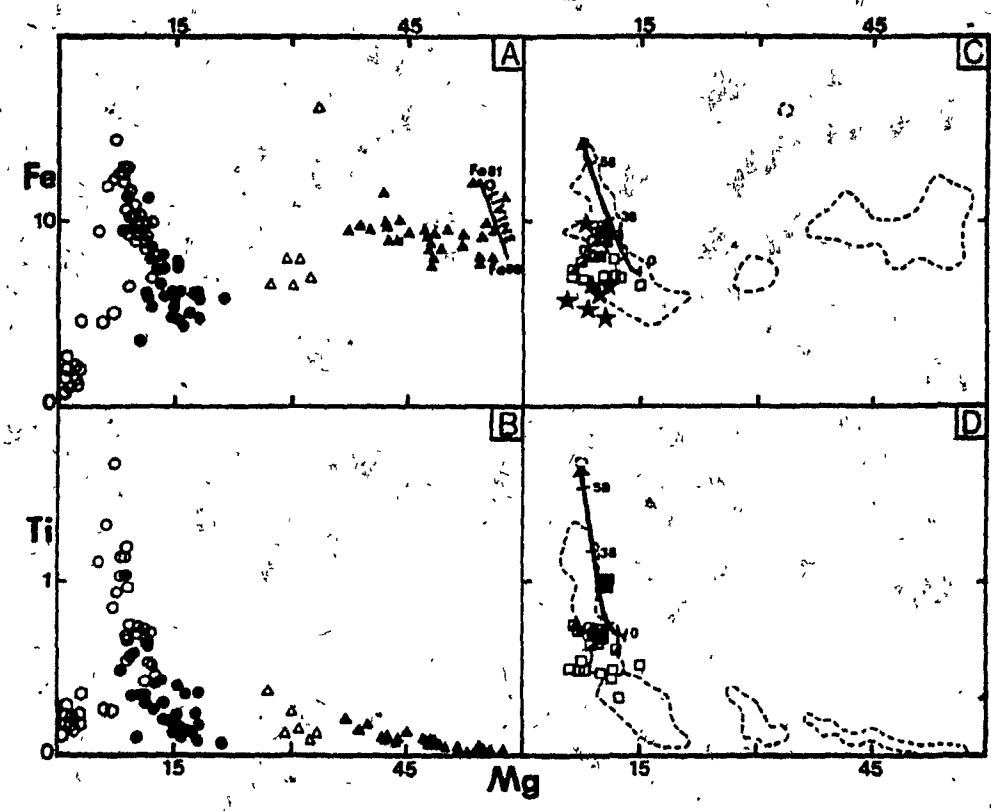

Table 3. Bulk XRF compositions of the Lac Yasinski intrusive rocks

Major and trace elements X-Ray fluorescence analysis were performed at McGill University, Montréal with a Phillips PW 1400. All elements with the exception of Zr and Y were determined from fused discs and corrected for mass absorption using an α coefficient technique (Ahmedali 1983). Total Fe is calculated as Fe2+. The analytical precisions (one standard deviation, weight percent) as calculated from 20 replicate analyses of one sample are: Si 0.05, Ti 0.003, Al 0.03, Mg 0.058, Fe 0.01, Mn 0.001, Ca 0.01, Na 0.06, K 0.001, P 0.004. Zr and Y were analysed from pressed pellets on which the detection limit is 5ppm. KB Compton scatter from the rhodium X-Ray tube was used to correct for mass absorption for these elements. The absolute precision is less than 5%.

	Contaminated gabbros		Fine-grained gabbros			Coarse-grained gabbros			Peridotites	
	84087	84098	83131	83084	84001	84146	84035	84128	84311	84029
SiO2	38.25	39.40	49.81	48.81	49.24	48.78	48.34	50.22	41.48	40.17
TiO2	0.61	0.44	0.77	0.89	1.29	0.10	0.25	0.30	0.12	0.10
Al2O3	14.30	13.89	14.75	14.97	13.55	13.62	15.25	13.21	4.39	4.53
MgO	5.82	5.84	8.34	8.30	5.51	15.34	13.07	10.55	28.92	30.14
FeO	8.49	6.74	10.90	11.06	15.47	7.53	7.86	7.96	11.88	10.95
MnO	0.18	0.14	0.20	0.21	0.26	0.16	0.17	0.18	0.12	0.17
CaO	6.36	5.45	11.16	10.57	9.67	9.28	9.29	14.66	1.81	2.62
Na2O	2.63	4.02	2.66	2.20	2.42	1.28	1.45	0.87	0.10	0.12
K2O	0.78	1.52	0.52	0.84	0.36	0.16	0.94	0.21	0.00	0.00
P2O5	0.07	0.34	0.05	0.05	0.10	0.01	0.02	0.03	0.01	0.02
LOI	2.66	1.58	0.99	1.92	1.54	3.85	3.46	1.94	10.20	10.50
Total	100.15	99.76	100.15	99.82	99.41	100.11	100.10	100.13	99.03	99.32
Cation units based on 100 cations										
Si	55.76	55.63	46.39	46.19	47.74	45.66	45.31	47.27	40.66	39.05
Ti	0.44	0.45	0.54	0.63	0.94	0.07	0.18	0.21	0.09	0.07
Al	14.13	15.33	14.19	14.70	15.48	15.02	14.85	14.65	5.07	5.19
Mg	8.30	8.15	11.58	11.71	7.96	21.40	18.26	14.80	42.25	43.67
Fe	6.80	5.28	8.49	8.75	12.54	5.90	6.16	6.27	9.74	8.90
Mn	0.15	0.11	0.16	0.17	0.21	0.13	0.13	0.14	0.10	0.14
Ca	6.92	5.67	11.14	10.72	10.04	9.31	9.33	14.78	1.90	2.73
Na	4.88	7.30	4.80	4.04	4.55	2.32	2.64	1.59	0.19	0.23
K	0.95	1.82	0.62	1.01	0.45	0.19	1.12	0.25	0.00	0.00
P	0.06	0.27	0.04	0.04	0.08	0.01	0.02	0.02	0.01	0.02
MgO	0.550	0.607	0.577	0.572	0.388	0.784	0.748	0.702	0.813	0.831
Ba	241	408	---	---	64	---	244	8		
Ir	85	134	65	---	95	34	42	46		
Y	18	19	18	---	31	4	8	10		

contents than the peridotites. In Mg-Fe space (Fig. 8a) they lie at Mg values intermediate between those of the peridotites and the Mg rich gabbros.

The gabbros as a whole define a pronounced Fe and Ti enrichment trend with decreasing Mg (Fig. 8a, 8) (Table 3). The majority of the coarse-grained gabbros plot at the high Mg end of the spectrum while the fine-grained gabbros dominate the low Mg end. In Al-Si space the gabbroic population displays a slight overall decrease in Al with rising Si (Fig. 9a). Incompatible elements such as Zr, Y, and Nb vary by a factor of approximately 1.7 across the spectrum of fine-grained gabbroic compositions. A small number of the fine-grained gabbros lie within the field of the coarse-grained gabbros (Fig. 8a) and are characterized by low values of Fe and Ti with respect to the majority of the fine-grained gabbros. Despite their low content in Fe and Ti these gabbros display low Al values and span a broad range of Si contents (46-50 cation %). The gabbros which contain felsic material differ from the main gabbro trend. They are commonly enriched in Si but depleted in Fe when compared to other gabbros at similar Mg# and they depart from the main gabbro spectrum towards the compositions of tonalite or sediment (Fig. 10a, b). These gabbros are enriched in Zr (Fig. 10c) with respect to gabbros without felsic inclusions.

The mafic volcanic rocks of this study range from basalt (SiO_2 < 52 wt %) to basaltic andesite (SiO_2 < 57 wt %)

Fig. 9: Al versus Si (cation units) for the Lac Yasinski gabbros (a) and basalts (b). Symbols as in Fig. 8a and b. The arrow indicated the fractional crystallization path (20% ol, 32% cpx, 48% plag) calculated for the fine-grained gabbros. Fractional crystallization was modelled using a finite-difference computer technique similar to that of Nathan and Van Kirk (1978) with modifications similar to those of Cox (1980). The fractional crystallization model consisted of the repeated calculation of the instantaneous equilibrium compositions of crystals coexisting with the liquid. Each step involved the removal of a quantity of these phases equivalent to 0.01 cation per cent of the initial parent, and the recalculation of the residual liquid to 100 per cent. The phase compositions were calculated from algorithms given by Hart and Davis (1978) and Ford et al. (1983) for olivine, Morse (1982) for plagioclase and Gamble and Taylor (1980) for clinopyroxene. The equilibrium temperature compiled for olivine at each step was used to define the Fe/Mg ratio of the clinopyroxene.

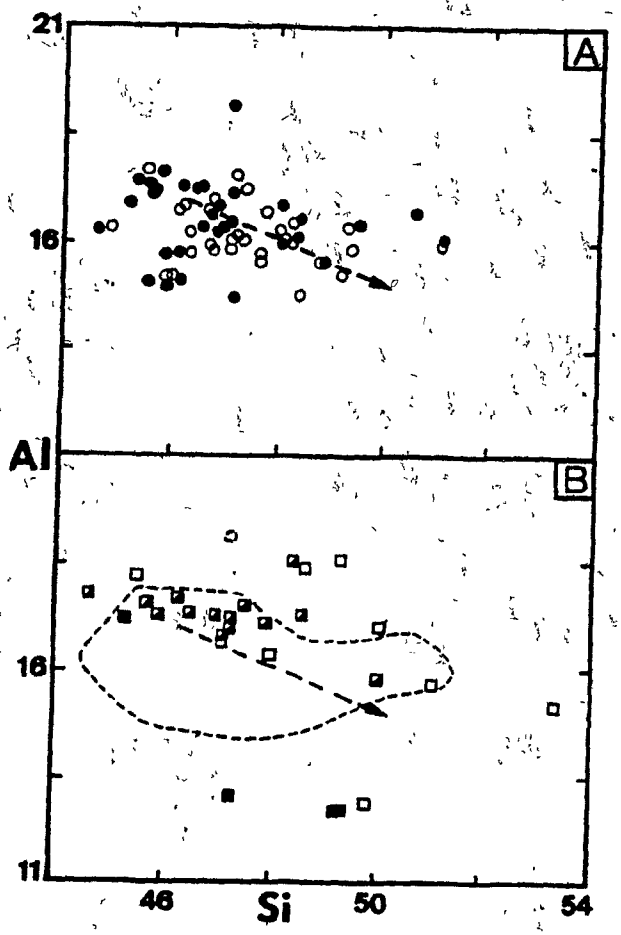

Fig. 10: Si, Fe (cation units) and Zr (ppm) versus Mg# for the contaminated and uncontaminated gabbros of Lac Yasinski. Symbols as in Fig. 8

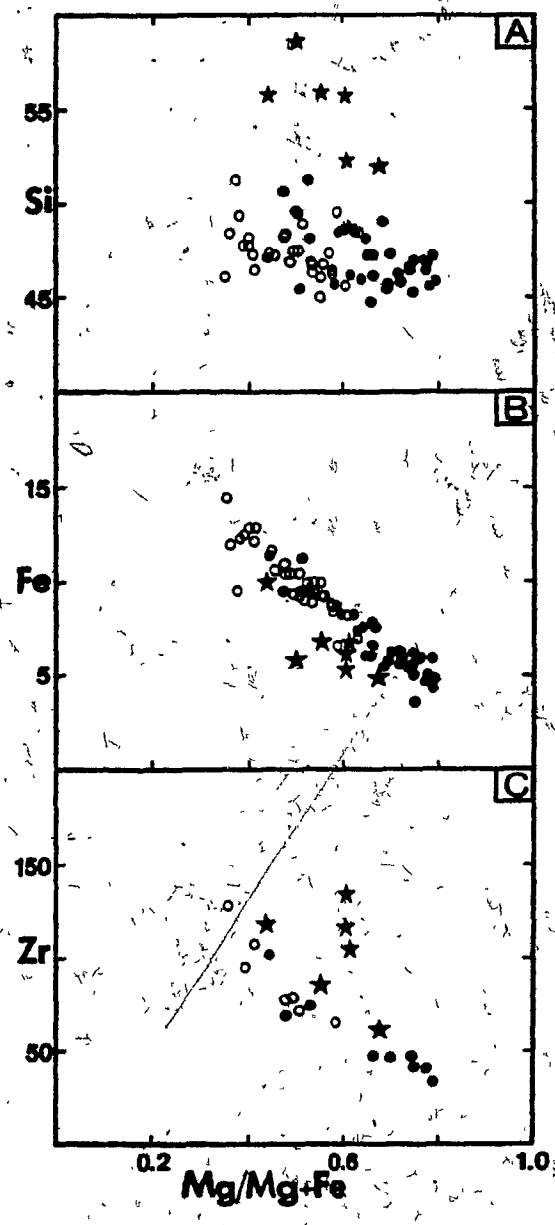

(Jolly 1975, Gélinas et al. 1984) in composition. The measured volcanic succession is comprised of three populations in terms of Ti content (Fig. 8d). The earliest lavas have intermediate Ti values (0.7 cation %) and are stratigraphically overlain by later lavas of lower Ti content (0.45 cation %) (Table 4). At the top of the stratigraphy, the four samples collected from the youngest flows are characterized by the highest Ti contents (0.98 cation %).

The intermediate-Ti lavas span a range of Si contents similar to that of the fine-grained gabbros. The low-Ti lavas span a even greater range of Si contents and are on the average more siliceous than the intermediate-Ti lavas. The high-Ti lavas appear to be anomalously poor in Al compared to the other lavas. There is considerable overlap between the compositions of the lavas and the gabbros (Fig. 8c and d) and both have generally similar Zr, Y, Nb, Ba and Rb abundances at similar Mg number. However, whereas the gabbros define an overall trend of increasing Fe, Ti and Zr with decreasing Mg, no such tendency is apparent within the lavas of any given Ti group. In fact some of the intermediate-Ti lavas appear to define a trend of Fe-depletion with decreasing Mg. The lavas in question are displaced towards higher Al and Si contents than the majority of the intermediate Ti lavas. Despite the absence of an Fe-enrichment trend, however, the lavas display a range in Si comparable to or exceeding that observed in the fine-grained gabbros.

Table 4. Bulk rock XRF analyses of the Lac Yasinski volcanics

All samples were taken from the chilled margins of pillows.

	Low-Ti lavas				Intermediate-Ti lavas		
	84163	20012	20013	83151	20002	20006	20010
SiO2	51.70	50.21	51.44	55.79	49.76	50.23	50.66
TiO2	0.71	0.63	0.68	0.68	0.95	0.97	1.02
Al2O3	14.91	14.96	16.41	13.39	15.30	15.13	16.44
MgO	8.29	8.18	5.42	5.66	7.05	5.12	4.65
FeO	9.07	10.22	8.58	10.17	11.59	9.61	9.08
MnO	0.21	0.20	0.18	0.25	0.18	0.18	0.17
CaO	10.73	12.34	13.55	10.82	11.59	13.41	12.83
Na2O	3.05	1.86	1.96	1.72	1.94	2.11	2.59
K2O	0.18	0.27	0.45	0.20	0.08	0.12	0.21
P2O5	0.05	0.04	0.05	0.04	0.07	0.06	0.07
LOI	0.70	0.97	1.07	1.59	0.79	2.85	2.47
Total	99.57	99.88	99.79	100.31	99.30	99.79	100.19
Cation units based on 100 cations							
Si	48.06	47.18	48.70	53.36	47.30	48.64	48.45
Ti	0.50	0.45	0.48	0.49	0.68	0.71	0.73
Al	16.34	16.57	18.31	15.09	17.14	17.27	18.53
Mg	11.49	11.46	7.65	8.07	9.99	7.39	6.63
Fe	7.05	8.03	6.80	8.13	9.21	7.78	7.26
Mn	0.17	0.16	0.14	0.20	0.14	0.15	0.14
Ca	10.69	12.42	13.74	11.09	11.80	13.91	13.15
Na	5.50	3.39	3.60	3.19	3.58	3.96	4.80
K	0.18	0.32	0.54	0.24	0.10	0.15	0.26
P	0.04	0.03	0.04	0.03	0.06	0.05	0.06
MgO	0.620	0.588	0.529	0.498	0.520	0.487	0.477
Ba	27	54	52	---	1	27	65
Zr	65	60	62	69	78	80	78
Y	19	17	18	18	24	25	25

5.7 Discussion

Chemical variations observed in Archean rocks may be a function of both primary compositional variation and secondary processes such as low-temperature alteration, burial and regional metamorphism and local metasomatism. It is difficult to assess rigorously the extent to which such secondary processes have modified magmatic compositional relationships. There is general agreement that large-ion-lithophile elements such as Na, K, Rb and Ba may be mobilized in metamorphic terrains (Hart 1969, Hart et al. 1970). As a consequence, classifications based on normative mineralogy must be dealt with caution and little weight can be given to these elements during modeling. There are conflicting results with respect to the mobility of elements such Ca and Al. In some greenstone localities they are reported to be enriched (Condie et al. 1977) and in others depleted (Jolly and Smith 1972) in comparison to expected magmatic values. In the Yasinski rocks Ca and Sr appear to display a positive correlation with volatile content suggesting these elements have been remobilized. On the other hand, elements with high field strength such as Ti, Zr and Y are claimed by many authors to be relatively immobile during greenschist metamorphism (Pearce and Cann 1973, Coish 1977, Ludden et al. 1982). In the Yasinski rocks, no correlation is observed between volatile content and these elements. The same observation is true for Mg, Fe and Si. These elements do not appear to have been strongly remobilized and thus may be used

to study the magmatic processes responsible for the Yasinski rocks.

The compositional field of the Lac Yasinski gabbros coincides with the spectrum of liquid compositions produced in low pressure melting experiments on a primitive MORB basalt (Spulber and Rutherford 1983), suggesting that they lie along a low pressure cotectic (Fig. 8c and d) involving plagioclase and pyroxene. The fine-grained gabbros may approximate liquid compositions, while the coarse-grained gabbros must in part represent cumulate compositions. A mixing program (Wright and Doherty 1970) was used to test whether the Fe-rich gabbros could have been derived by crystal fractionation from a parent representing an average of the Mg-rich, fine-grained gabbros adjacent to the field of the coarse-grained gabbros. The most successful models involved the removal of an assemblage composed of plagioclase, clinopyroxene and olivine (in proportions of 48%, 32% and 20% respectively). Over 50 % crystallization is required to produce the entire spectrum of fine-gabbro compositions to its most iron-rich members. There was a good agreement between the amount of fractionation predicted by such models and that estimated on the basis of the variation of highly incompatible elements such as Zr.

Most of the mafic lavas of the Lac Yasinski belt cluster with the gabbros of the intrusion along a trend of slightly decreasing Al with increasing Si (Fig. 9a, b), a

feature characteristic of magmas along a plagioclase saturation surface. However, the spread in Si of the low-Ti lavas cannot be reproduced by gabbroic crystallization models involving plagioclase, clinopyroxene, and olivine. The extent of fractionation required by such models to account for the Si variation produces a sharp rise in Ti and Fe which is not observed in the low-Ti lavas. The crystallization of reasonable amounts of chromite and the calculation of a portion of Fe as Fe_2O_3 reduces the discrepancy, but are still incapable of preventing the buildup of Fe. Similar problems are encountered when trying to model the compositional variation within the intermediate-Ti lavas. The situation becomes worse when gabbroic fractionation models are used to try to derive the intermediate-Ti lavas from the more primitive low-Ti lavas because the increase in Si which such models produce is inconsistent with the lower Si content of the intermediate-Ti lavas with respect to the low-Ti lavas.

There is no evidence to suggest that alteration is responsible for the Si difference observed between these two stratigraphically and chemically distinct lava suites of Lac Yasinski. The presence of tonalitic xenoliths in some gabbroic dykes indicates the possible role of contamination in producing Si enrichment. These xenolith-bearing gabbros display a marked increase in Si, Ba/Zr, and Zr/Y ratios and decrease in Fe with respect to other gabbros of similar Mg# (Fig. 10a, b) (Table 3) which can be attributed to the

assimilation of tonalite. Although some low-Ti Yasinski lavas have similar Ti, Fe and Mg contents to the contaminated gabbros (Fig. 8c and d), they have distinctly lower Zr, Rb and Ba contents (Fig. 10c) (Table 4). These chemical features suggest that the high Si content of the low-Ti lavas is not the result of contamination and indicates that the difference in silica between low-Ti and intermediate-Ti lavas reflects a fundamental difference in their fractionation histories which precludes deriving one from the other.

Although no lavas more primitive than basalts are observed at Lac Yasinski, the olivine dominated cumulate of the layered intrusion implies the existence of more primitive magmas. Primitive komatiitic lavas have erupted with basalts in the eastern Lac Guyer segment of the La Grande belt (Fig. 6). St-Seymour et al. (1983) have proposed that the basalts of the Lac Guyer area were derived by crystal fractionation in subcrustal magma chambers from parental magmas which were compositionaly equivalent to the associated komatiitic lavas. As the basalts of the Lac Guyer segment fall along the compositional spectrum of the Yasinski gabbros and cluster with those of the Lac Yasinski lavas, the komatiites and komatiitic basalts of Lac Guyer may also provide compositional analogues of the parental magmas to the lavas of the Lac Yasinski segment of the La Grande greenstone belt. At Lac Guyer, the compositional field of basaltic lavas is linked to that of the komatiites by that of less abundant komatiitic or picritic basalts. The distribution of these

lavas in Al-Si space (Fig. 11a) suggests that they were fractionating along an olivine-pyroxene cotectic (Seymour and Francis 1986). The fact that Ca does not decrease in these lavas indicates the pyroxene was predominantly orthopyroxene. The best models for this trend require more than 50% fractionation of an assemblage composed of orthopyroxene and olivine (57 and 43% respectively Fig. 11b path a) for komatiitic parental magmas to evolve to compositions similar to those of the basalts. A pressure on the order of 10kb would be required to eliminate the olivine+orthopyroxene reaction relationship (Takahashi and Kushiro 1983) to enable such a model to work. In support of such a model, the Lac Guyer komatiitic basalts define a path of constant normative quartz in an Ol+Qtz+Plag liquidus projection (Fig. 12) which follows the experimentally determined positions of the olivine+orthopyroxene cotectic between 10 and 25 Kb (Elthon et al. 1984).

If the Lac Yasinski basalts and gabbros were derived from komatiitic parental magmas undergoing a similar fractionation history, then a mechanism presents itself for explaining the behaviour of Si in the Lac Yasinski lavas. The primary phase volume of olivine expands with decreasing pressure (O'Hara 1968) and in Al-Si space (Fig. 11a) the position of the olivine+orthopyroxene cotectic would shift towards higher Si values. The low-Ti lavas of the Lac Yasinski segment of the La Grande greenstone belt may have evolved from residual liquids tapped at various stages of

Fig. 11: a Al versus Si (cation units) for the Lac Guyer basalt-komatiite suite. Basalts, open circles; komatiites, solid circles. b Al versus Si (cation units) for the Lac Yasinski lavas. Symbols as in Fig. 8c and d. The continuous line marks the field of the Lac Yasinski gabbros. The dashed line marks the field of the Lac Guyer basalt-komatiite suite displayed in Fig.11a. The arrows indicate fractional crystalization paths calculated with the following phase assemblages: arrow a= 57% opx, 43% ol; arrow b-b'' = oliv; arrow c-c''' = 60% cpx, 40% plag.

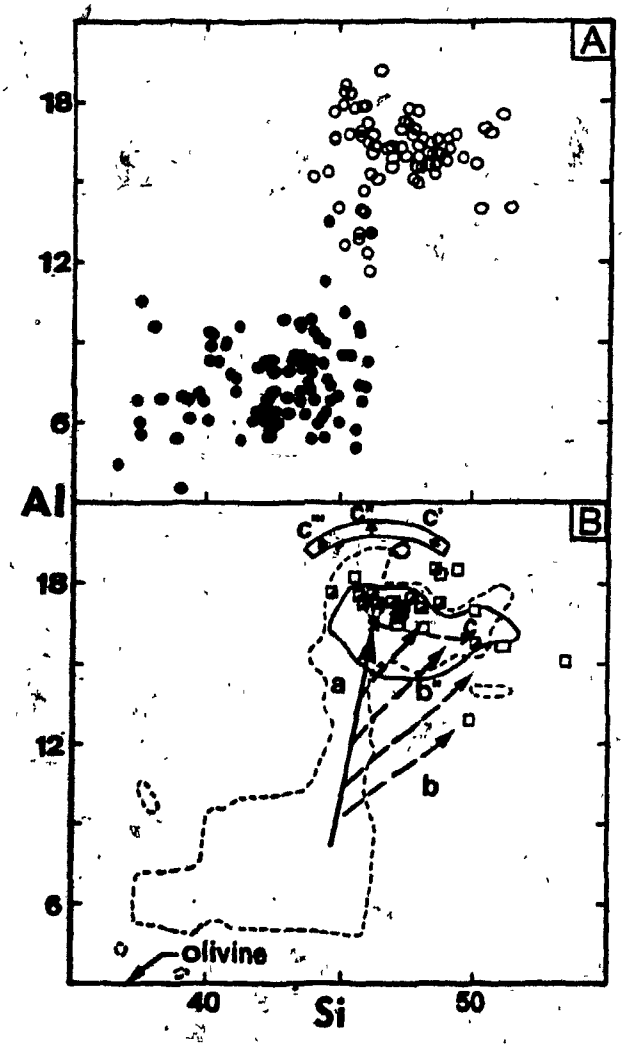

Fig. 12: Olivine-silica-plagioclase isomolar liquidus projection for the Lac Guyer basalt-komatiite suite. Symbols as in Fig. 8. The experimentally determined cotectic boundaries are taken from Elthon et al. 1984. 1=1atm, 2=10Kb, 3=20Kb, 4=25Kb.

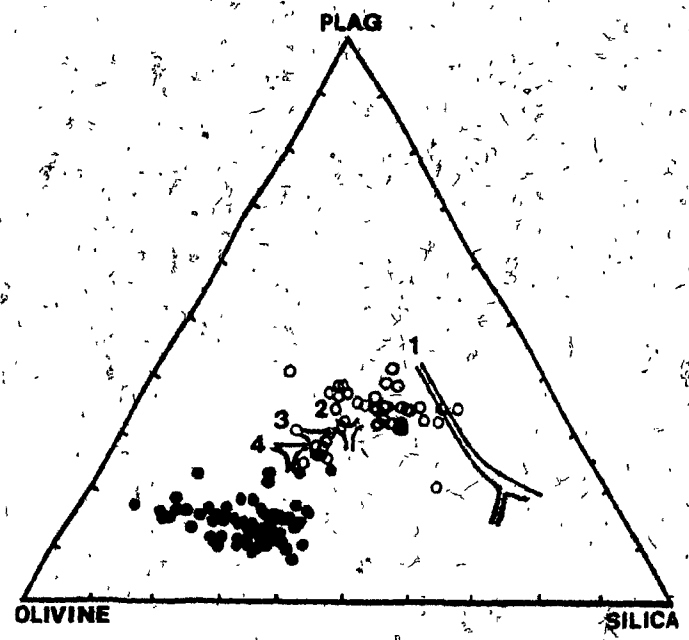

high pressure fractionation along an olivine+orthopyroxene cotectic. As these magmas rose to the surface, the expansion of the olivine liquidus volume would have caused them to become supersaturated with respect to olivine and to fractionate along a series of olivine control lines (Fig. 11b paths b through b''). This mechanism would account for the spread in Si and Al contents of the Lac Yasinski lavas at relatively constant Ti, P, Zr and Fe. The olivine cumulate of the Lac Yasinski intrusion may represent the mineral extract from these picritic liquids fractionating along olivine control lines as they rose to the surface. A similar scenario has been proposed by Jamieson (1966, 1970) and later by Cox and Jamieson (1973) for the olivine-rich basalts of the Karroo province. The higher Al content (Fig. 9b) and lower Mg content (Fig. 8c, d) of some of aphyric low-Ti basalts with respect to the gabbros suggests that these magmas failed to nucleate plagioclase and overshot the plagioclase-pyroxene cotectic defined by the spectrum of gabbro compositions (Fig. 8a). This would explain why these lavas show no signs of iron enrichment.

The lower Si content of the intermediate-Ti basalts indicates that they were derived from magmas which had experienced larger extents of high-pressure olivine+orthopyroxene fractionation than those which gave rise to the low-Ti lavas. Such residual magmas would reach Al-rich compositions which would be saturated with respect to plagioclase and pyroxene rather than olivine when they

finally rose to low pressures. They would thus undergo gabbroic fractionation rather than olivine fractionation within the low pressure conduit system. In this region of Al-Si space, however, calculations using algorithms from Morse (1982) and Gamble and Taylor (1980) indicate that for a small decrease in Si content, the composition of the bulk gabbroic cumulate changes from being less siliceous to more siliceous than that of the corresponding magma. A fan-like array of gabbroic fractionation paths exists in this region of Al-Si space (Fig. 11b path c-c'''). Consequently the low pressure fractionation path of such magmas is strongly sensitive to the Si content produced by the previous history of high pressure fractionation. The spectrum of intermediate-Ti lavas could simply represent the locus of this array of gabbroic fractionation trends, while the coarse-grained gabbros of the Lac Yasinski intrusion would represent the extracted cumulate.

The high-Ti lavas exposed at the upper levels of the stratigraphy display anomalously low Al contents but have the highest Ti and Zr contents of the Lac Yasinski basalts. It is difficult to postulate a mechanism which could derive these lavas from magmas equivalent to the low or intermediate-Ti lavas. These observations are based on the analysis of four samples and alteration may be a problem.

Some of the intermediate-Ti Yasinski basalts appear to define a trend of iron depletion (Fig. 8c) in Mg-Fe space.

However, the lack of variations of the Ti and Zr along this trend and the higher Al and Si in the lavas which define it suggest that the nature of this trend was a function of different extents of olivine+orthopyroxene fractionation at high pressure. Extensive degrees of fractionation at high pressure resulted in gabbroic fractionation at low pressure and produced basalts of relatively higher Fe content. Smaller degrees of olivine+orthopyroxene fractionation at high pressure lead to excess olivine fractionation at low pressure which produced evolved basalts without Fe-enrichment. A spectrum of these combined processes could produce the locus of basalt compositions which appears to define an Fe-depletion trend. The gabbros of the Lac Yasinski intrusion which contain felsic material on the other hand define a definite trend of iron depletion in Mg-Fe space (Fig. 8c) and depart from the main gabbro spectrum towards the composition of tonalite. This indicates that the assimilation of tonalitic contaminant was responsible for the iron depletion in these rocks. Although no lavas corresponding to the contaminated gabbros have yet been recognized in the Yasinski segment of the La Grande greenstone belt, the second cycle volcanics, described by Skulski (1985) may represent the extrusive equivalents of the contaminated gabbros.

5.8 Conclusions

The Lac Yasinski intrusion represents a relic of a shallow level magma conduit emplaced at the base of a greenstone succession. It records the operation of the low

pressure fractionation processes which have affected the evolution of magmas in the Lac Yasinski greenstone belt. The coarse grained gabbros of the Lac Yasinski intrusion represent cumulates of material extracted from the parental magma which produced the intermediate-Ti lavas. The peridotite appears to represent the olivine cumulate extracted from more primitive magmas which were supersaturated with olivine and yielded the low-Ti Lac Yasinski lavas. The cross cutting relationship of related dykes suggest magmas of the conduit system became more mafic with time. The general absence of gabbros cutting the peridotite suggests that the magmas which formed the olivine cumulate came later than those which produced the bulk of the gabbro dykes and cumulates. This agrees with the stratigraphy of the Lac Yasinski segment of the La Grande greenstone belt which indicates that the intermediate-Ti basalts were extruded first followed by a voluminous outpouring of low-Ti basalts. The models developed in this paper suggest that this evolution can be understood in terms of decreasing residence time of magmas in high pressure chambers. In the early stages of volcanism, magmas underwent extensive fractionation of olivine and orthopyroxene at high pressures which produced high Al contents at low Si. The evolved residual magmas reached compositions which were close to plagioclase and clinopyroxene saturation when they rose from depth and underwent gabbroic fractionation in shallow level conduit systems before erupting as the intermediate-Ti

lavas. As the magmatic plumbing system evolved, magmas were tapped from their high pressure fractionation sites at earlier stages in their evolution and reached the shallow level conduit system supersaturated in olivine. These magmas fractionated along olivine control lines and produced the olivine cumulates of the Lac Yasinski intrusion before they erupted as the low-Ti lavas. The delayed crystallization of plagioclase in these magmas resulted in an overshooting of the plagioclase-pyroxene cotectic and the absence of an Fe-enrichment trend. In the eastern Lac Guyer segment of the La Grande greenstone belt, komatiitic magmas were eventually able to reach the surface having experienced essentially no high pressure crystallization (St-Seymour et al, 1983).

The basalts and contaminated gabbros of the Lac Yasinski segment illustrate different mechanisms for the generation of iron-depletion trends. The intermediate Ti basalts exhibit an apparent iron depletion trend. Their chemical pattern can be understood in terms of different extents of high pressure fractionation which determined the nature of the low pressure fractionating assemblage of the magma. Magmas which fractionated olivine at low pressure and failed to nucleate placioclase display low Mg and Fe contents. Magma evolution dominated by gabbroic fractionation at low pressure evolve towards higher Fe contents. A spectrum of basalts which have fractionated along paths between these limits will produce a locus of compositions which define an apparent Fe-depletion trend. The contaminated

gabbros of the Lac Yasinski intrusion display a real Fe depletion trend due to the assimilation of granitic crust by basaltic magma. The general tendency of Fe-depletion trends to dominate in the later stages of greenstone volcanism may reflect the increasing interaction of basaltic magma with crustal material with time.

6 SUMMARY, IMPLICATIONS, AND RECOMMENDATIONS FOR FURTHER WORK

The preceeding manuscript documented the complex interplay of processes involved in the evolution of mafic magmas in the Lac Yasinski segment of the La Grande greenstone belt. In particular, the behaviour of Fe in such magmas was shown to be a sensitive function of their fractionation history. Prolonged residence of magmas at high pressure produced compositions which were saturated with plagioclase at low pressure. Extensive gabbroic fractionation of such magmas at shallow levels produced residual liquids which evolved towards Fe-rich compositions. Magmas which attained crustal levels with relatively primitive compositions however were supersaturated in olivine and underwent excess olivine fractionation to produce residual magmas without a rise in Fe content. Magmas which assimilated crustal material on their way to the surface evolved towards Fe-poor compositions. In the Lac Yasinski segment of the La Grande greenstone belt each of these divergent trends appear to have developed from a common parental magma composition in response to different fractionation histories.

A common approach in studies of Archean petrogenesis involves the use of AFM projections to discriminate volcanic suites of tholeiitic and calc-alkaline affinities. Such diagrams are commonly used to interpret Archean volcanic suites in terms of modern plate tectonic models. In figure 13 the fine-grained gabbros, lavas, and contaminated gabbros

Fig. 13: AFM plot (in weight %) of the bulk compositions of the fine-grained gabbros, contaminated gabbros and lavas of the Lac Yasinski segment. Symbols as in Fig. 8. Tholeiite boundary line after Irvine and Baragar (1971).

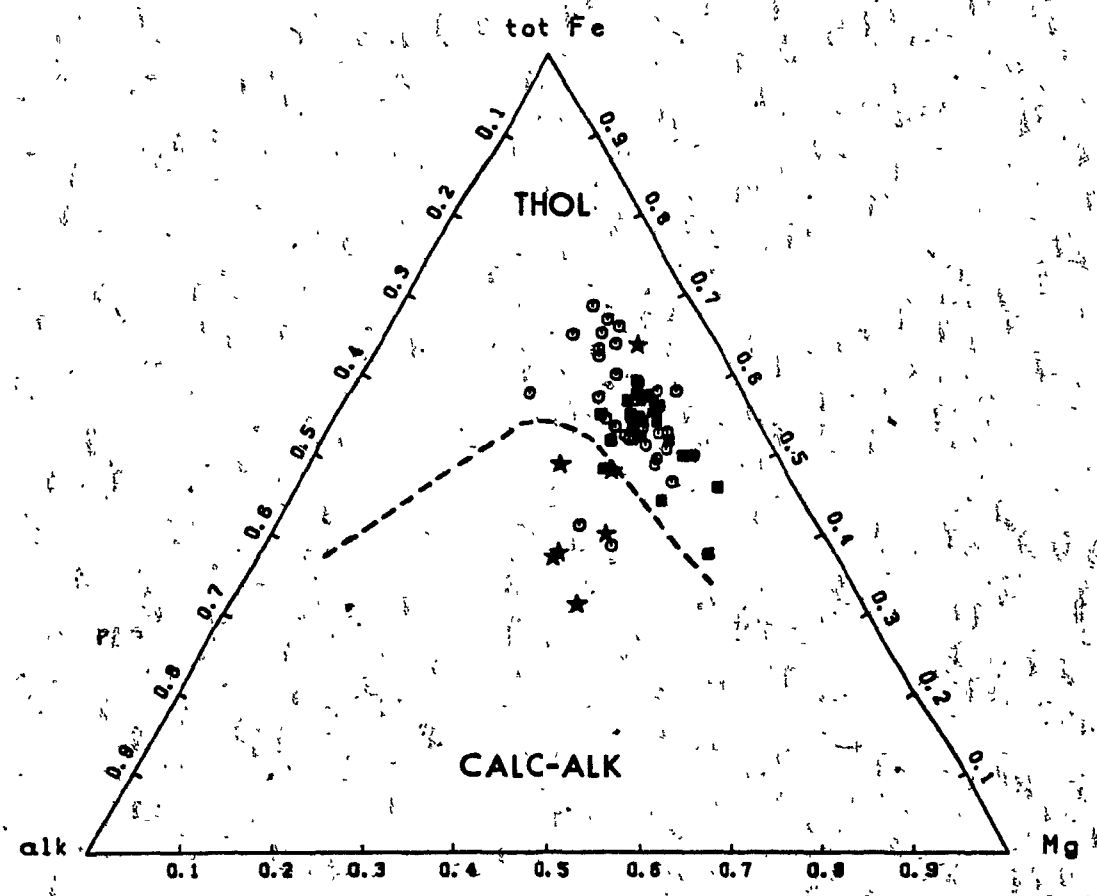

of the Lac Yasinski segment of the La Grande belt are plotted in an AFM diagram. The fine-grained gabbros and lavas fall within the tholeiite field while the contaminated gabbros plot in the field of calc-alkaline rocks. This illustrates that studies of Archean basalt petrogenesis which rely simply on AFM projections may neglect important aspects of the basalt evolution history and emphasizes that plate tectonic interpretations based on such diagrams should be viewed with caution.

The results of this thesis emphasize the value of comparing associated extrusive and intrusive rocks to the study of the processive controlling the petrogenetic evolution of lavas. The postulation that the process of contamination observed in the gabbroic dykes is responsible for Fe-depletion trends in Archean lavas could ~~not be~~ tested because the absence of such lavas in the study area of the Lac Yasinski segment of the La Grande greenstone belt. This hypothesis needs to be tested in a greenstone belt in which a mafic intrusive complex occurs in close spatial relationship with a succession of lavas characterized by an Fe-depletion trend. The study of such an association would improve our understanding of the development of Fe-depletion trends in the lavas of the upper portion of Archean greenstone belts.

REFERENCES

Ahmedali T (1983) XRF procedures, circular #1, Dept Geological Sciences, McGill University

Arndt NT (1977) Ultrabasic magmas and high-degree melting of the mantle. Contr Mineral Petrol 64:205-221

Arndt NT, Naldrett AJ, Pyke DR (1977) Komatiitic and iron-rich tholeiitic lavas of Munro township, Ontario: trace element evidence. Geology 5:590-594

Baragar WRA (1966) Geochemistry of the Yellowknife volcanic rocks. Can J Earth Sci 3:9-30

Baragar WRA (1968) Major element geochemistry of the Noranda volcanic belt, Quebec-Ontario. Can J Earth Sci 5:773-790

Bickle MJ, Bettenay LF, Barley LF, Chapman HJ, Groves DI, Campbell IH, De Laeter JR (1983) A 3500 Ma plutonic and volcanic calc-alkaline province in the Archean East Pilbara block. Contr Mineral Petrol 84:25-35

Ciesielski A, (1984) Géologie de la Grande Rivière (Chissassibi-LG3) sous province de la Baie James, Québec. Geol Surv Canada, open file Map 379

Coish RA (1977) Ocean floor metamorphism in the Betts Cove ophiolite, Newfoundland. Contr Mineral Petrol 80:255-70

Condie KC (1976) Trace-element geochemistry of Archean greenstone belts. Earth Sci Rev 12:393-417

Condie KC Viljoen MJ and Kable EDJ (1977) Effects of alteration on element distributions in Archean tholeiiites from the Barberton greenstone belt, South Africa. Contr Mineral Petrol 64:75-89

Condie KC, (1981) Archean greestone belts: Elsevier, Amsterdam, 432 p

Cox KG, Jamieson BG (1974) The olivine-rich lavas of Nuanetsi: a study of polybaric magmatic evolution. J Petrol 15:269-301

Cox KG (1980) A model for flood basalt volcanism. J Petrol 21:629-50

Davis Jr PA, Condie KC (1977) Trace element model studies of Nyanzian greenstone belt, western Kenya. Geochim Cosmochim Acta 40:271-277

Donaldson CH, (1976) An experimental investigation of olivine morphology. Contr Mineral Petrol 57:187-213

Eade KE, (1966) Fort George river and Kaniapiskau river (West-half) map-areas, New Quebec, Geol Surv Canada Memoir 339

Elthon D, Scarfe CM (1984) High-pressure phase equilibria of a high-magnesia basalt and the genesis of primary oceanic basalts. Am Mineral 69:1-15

Ford CE, Russell DG, Craven JA, Fisk MR (1983) Olivine-liquid equilibria: temperature, pressure and composition of the crystal/liquid cation partition coefficient for Mg, Fe2+, Ca and Mn. J Petrol 24:256-265

Fouques JP, Schumacker F, (1979) Rapport de synthèse du permis SES, SERU Nucléaire, Eldorado Nucléaire, SDBJ, 26 p

Gamble RP, Taylor LA (1980) Crystal/liquid partitioning in augite: effects of cooling rate. Earth Planet Sci Lett 47: 21-33

Gélinas L (1984) Chemostratigraphic division of the Blake River group, Rouyn-Noranda area, Abitibi, Québec. Earth Planet Sci Lett 23:220-231

Goodwin AM (1977) Archean volcanism in Superior province, Canadian shield. Geol Assoc Canada Spec Paper 16:205-241

Hart SR (1969) K, Rb, Cs contents and K/Rb and K/Cs ratios of fresh and altered submarine basalts. Earth Planet Sci Lett 6:295-303

Hart SR, Brooks C, Krogh TE, Davis GL and Nava D (1970) Ancient and modern volcanic rocks: a trace element model. Earth Planet Sci Lett 10:17-28

Hart SR, Davis KE (1978) Nickel partitioning between olivine and silicate melt. Earth Planet Sci Lett 40:203-219

Hawkesworth CJ, O'Nions RK (1977) The petrogenesis of some Archean volcanic rocks from southern Africa. J Petrol 18:487-520

Irvine TN, Baragar WRA (1971) A guide to the chemical classification of the common volcanic rocks. Can J Earth Sci 8:523-548

Jackson ED (1961) Primary textures and mineral associations in the ultramafic zone of the Stillwater Complex of Montana. US Geol Surv Prof Paper 358, 106p

Jahn BM, Auvray B, Blais S, Capdevila R, Cornichet J, Vidal P, Hameurt J (1980) Trace element geochemistry and petrogenesis of Finnish greenstone belts. J Petrol 21:201-244

Jamieson BG (1966) Evidence on the evolution of basaltic magmas at elevated pressures. Nature Lond 212:243-246

Jamieson BG (1970) Differentiation of ascending magma. In Newall G, Rast N (eds) Mechanism of igneous intrusion. Geological Journal Special Issue 2, Liverpool

Jolly WT, Smith RE (1972) Degradation and metamorphic differentiation of the Keweenawan tholeiitic lavas of northern Michigan, USA. J Petrol 13:273-309

Jolly WT (1975) Subdivision of the Archean lavas of the Abitibi area, Canada, from Fe-Mg-Ni-Cr relations. Earth Planet Sci Lett 27:200-210

Jolly WT (1977) Relations between Archean lavas and intrusive bodies of the Abitibi greenstone belt, Ontario-Québec. In Baragar WRA, Coleman LC, Hall JM (eds) Volcanic regimes in Canada. Geol Assoc Canada Spec Paper 16, pp. 311-330

Jolly WT (1980) Development and degradation of Archean lavas, Abitibi area, Canada, in light of major element geochemistry. J Petrol 21:323-363

Kuno H (1950) Petrology of Hakone volcano and the adjacent areas, Japan. Geol Soc Am Bull 61:957-1020

Kuno H (1968) Origin of andesite and its bearing on the island arc structure. Bull Volcanol 32:141-176

Kushiro I, Sato H (1978) Origin of calc-alkaline andesite in the Japanese islands. Bull Volcanol 41:576-585

Langmuir CH, Hansen GN (1980) An evaluation of major element heterogeneity in the mantle sources of basalts. Phil Trans R Soc Lond 297:383-407

Liu M (1985) Migmatization and volcanic petrogenesis in the La Grande greenstone belt, Québec. Unpublished Masters thesis, McGill University, Montréal, Québec, 87p

Ludden JN, Gelinas L, Trudel P (1982) Archean metavolcanics from the Rouyn-Noranda district Abitibi. Part II. Mobility of trace and rare earth elements. Can J Earth Sci 19:2276-2287

Masuda A, Aoki K (1979) Trace element variations in the volcanic rocks from the Nasu zone, northeast Japan. Earth Planet Sci Lett 44:139-149

Mills JP (1974) Petrological studies in the Sakami-Lake Greenstone belt of northwestern Québec. PhD Thesis, University of Kansas, Lawrence, Kansas, USA

Morse SA (1982) Plagioclase fractionation and the common basalt. J Geology 90:559-563

Nathan HD , Van Kirk CK (1978) A model of magmatic crystallization. J Petrol 19:66-94

O'Hara MJ (1968) The bearing of phase equilibria studies in synthetic and natural systems on the origin and evolution of basic and ultrabasic rocks. Earth Sci Rev 4:69-133

O'Nions RK, Pankhurst RJ (1978) Early Archean rocks and geochemical evolution of the earth's crust. Earth Planet Sci Lett 38:211-236

Osborn EF (1959) Role of oxygen pressure in the crystallization and differentiation of basaltic magma. Am J Sci 257:609-647

Pearce JA, Cann JR (1973) Tectonic setting of basic volcanic rocks determined using trace elements analyses. Earth Planet Sci Letters 19:290-300

Ringwood E (1977) Petrogenesis in island-arc system. In island-arcs, deep-sea trenches and back-arc basins (M Talwani and WC Pitman III, eds), Maurice Ewing series no 1, American geophysical union, Washington DC, 355-365

Roeder PL, Emslie RF (1970) Olivine-liquid equilibrium. Contr Mineral Petrol 29:275-289

Roeder PL (1974) Activity of iron and olivine solubility in basaltic liquids. Earth Planet Sci Lett 23:397-410

Sharma KNM (1977) Région de La Grande Rivière area: Ministère des Richesses Naturelles, Québec, Rapport géologique 184, 75p

Skulski T, Hynes A, Francis D (1984) Stratigraphic and lithogeochemical characterization of cyclic volcanism in the LG3 area; La Grande River greenstone belt, Québec. In Chibougamau-Stratigraphy and Mineralization, CIM Special Vol 34:57-72

Skulski T (1985) Unpublished MSc Thesis, McGill University, Montréal, Québec, 223p

Spulber SD, Rutherford MJ (1983) The origin of rhyolite and plagioagranite in oceanic crust: an experimental study. J Petrol 24:1-25

Stamatelopoulou-Seymour K (1982) Volcanic petrogenesis in the Lac Guyer greenstone belt, James Bay area, Québec. Unpublished PhD thesis, McGill University, Montréal, Québec, 304p

Stamatelopoulou-Seymour K, Francis D, Ludden J (1983) The petrogenesis of the Lac Guyer komatiites and basalts and the nature of the komatiite-komatiitic basalt compositional gap. Contr Mineral Petrol 84:6-14

Stamatelopoulou-Seymour K, Francis D (1986) The interaction between Archean mantle and crust, La Grande greenstone belt, New Quebec, Canada. Submitted to Precamb Res

Sun S, Nesbitt RW (1978) Petrogenesis of Archean ultrabasic and basic volcanics: evidence from rare earth elements. Contr Mineral Petrol 65:301-325

Takahashi E, Kushiro I (1983) Melting of a dry peridotite at high pressures and basalt magma genesis. Am Mineral 68:859-878

Taylor Sr, Hallberg JA (1977) Rare-earth element in the Marda calc-alkaline suite: an Archean geochemical analogue of Andean-type volcanism. Geochim Cosmochim Acta 41:1125-1129

Viljoen MJ, Viljoen RP (1969,) The geology and geochemistry of the lower ultramafic unit of the Onverwacht Group and a proposed new class of igneous rocks. Upper Mantle Project Geol Soc S Africa Spec Publ 2:221-224

Viljoen MJ, Viljoen RP (1970) Archean volcanicity and continental evolution in Barberton region, Transval. In African magmatism (TN Clifford and I Gass, eds), Oliver and Boyd, Edinburgh, 27-49

White D, McBirney AR (1979) Some quantitative aspects of orogenic volcanism in the Oregon Cascades. Geol Soc Am Mem 152:369-388

Wicks FJ, Whittaker, EJW (1977) Serpentine textures and serpentinization. Can Mineral 15:459-488

Worst BG (1958) The differentiation and structure of the Great Dyke of southern Rhodesia. Trans Geol Soc S Afr 61: 283-354

Wright TL, Doherty PC, (1970) A linear programming and least squares computer method for solving petrologic mixing problems. Bul Geol Soc Am 81:1955-2008

APPENDIX A

Analytical procedures and sample preparation

One hundred and fifty-three samples were submitted for major element determination. Thin sections were prepared for most of these samples in order to examine the extent of alteration. The samples were crushed, powdered and homogenised to -200 mesh in a tungsten carbide ring grinder. A smaller population (sixty-six samples) was analysed for selected trace elements.

All the major and trace element concentrations were determined by X-ray fluorescence, using a Philips PW-1400 spectrometer with a 100 KV generator at the Department of Geological Sciences, McGill University, Montréal. A calibration curve for the major and trace elements was derive by linear regression using 20 to 30 international reference materials (Ahmedali, S.T. 1983). Ba, V, Cr, Ni and major element analysis were determined from fused beads and corrected for mass absorption using an α coefficient technique. Total Fe is calculated as Fe_2O_3. The trace element detection limit for fused beads (Ba, V, Cr and Ni) is 10 ppm. The analytical precisions (one standard deviation, weight percent) for the major elements as calculated from 20 replicate analyses of one sample disc are: Si 0.05, Ti 0.003, Al 0.03, Mg 0.058, Fe 0.01, Mn 0.001, Ca 0.01, Na 0.06, K 0.001, P 0.004.

KB Compton scatter from the Rhodium X-ray tube was used to correct for mass absorption for the trace elements Rb, Sr, Zr, Y and Nb. These elements are analysed using pressed pellets for which the detection limit is 5 ppm. The absolute precision of all trace element data is generally better than 5% absolute (T. Ahmedali pers. comm. 1985).

For major element determination one gram of rock powder was mixed with five grams of lithium tetraborate, 0.3 gram of lithium flouride, 0.01 gram of ammonium nitrate and 0.015 gram of lithium bromide. The mixture was fused at 1050° C for 20 minutes in platimum crucibles and bound in polished Pt molds. The glass bead obtained was analysed for major elements and Ba, Ni, Cr and V determination. The loss on ignition technique served to approximate the volatile content of the rocks. For LOI determination two grams of rock powder was ignited at a temperature of 1000° C for a period of 45 minutes after which the difference between final weight and initial weight was determined and used to estimate the percent total volatile content of the rock. The pressed pellets were used for the determination of Zr, Y, Nb, Rb and Sr and obtained by mixing 8.000g of rock powder with 0.700g of thermosetting resin binder in a SPEX mixer for 5 minutes, and bound into pressed pellets at a pressure of 25 tons. These pellets were then cured in a drying oven at 200° C for 15 minutes.

APPENDIX B

Whole rock geochemistry

The analyses are presented in two formats. On each page the top format lists analyses in weight % which have not been normalized and includes loss on ignition. Total iron was calculated as Fe^{2+}. The lower format is in cation proportions based on 100 cations. The trace elements are in ppm.

Legend	Key
Perid.	peridotite
FineGb.	fine-grained gabbro
CoarGb.	coarse-grained gabbro
ContGb.	contaminated gabbro
LTiLav.	low-Ti lava
ITiLav.	intermediate-Ti lava
HTiLav.	high-Ti lava
Tonal.	tonalite

___ = concentrations not determined

Lagrande Yasinski

SAMPLE	84024 Perid	84026 Perid	84027 Pyrox	84029 Perid	84311 Perid	84312 Perid	84033 Pyrox	84050 Pyrox	84056 Perid	84114 Pyrox	41453 Pyrox	41454 Perid	41455 Perid	84166 Perid
SiO2	44.84	40.34	46.71	40.17	41.48	41.29	50.86	47.25	40.34	48.17	50.71	37.54	39.45	38.94
TiO2	0.20	0.13	0.12	0.10	0.12	0.12	0.18	0.21	0.28	0.53	0.36	0.23	0.18	0.07
Al2O3	4.25	3.97	6.85	4.53	4.39	4.37	4.16	6.79	5.83	8.28	3.99	4.12	4.29	1.88
MgO	26.70	29.90	23.04	30.14	28.92	28.55	20.94	22.10	25.48	19.44	21.43	26.00	30.62	34.56
FeO	11.99	12.08	8.76	10.95	11.88	11.93	10.19	10.10	11.54	8.46	8.25	11.05	11.34	11.66
MnO	0.20	0.19	0.22	0.17	0.12	0.12	0.21	0.26	0.23	0.22	0.21	0.17	0.15	0.07
CaO	2.33	1.27	7.95	2.62	1.81	1.79	10.00	8.37	5.98	8.53	10.45	5.70	0.96	0.01
Na2O	0.05	0.01	0.10	0.12	0.10	0.0	0.03	0.09	0.16	0.43	0.08	0.0	0.0	0.0
K2O	0.0	0.0	0.0	0.0	0.0	0.0	0.0	0.01	0.02	1.83	0.01	0.0	0.0	0.0
P2O5	0.02	0.02	0.01	0.02	0.01	0.01	0.02	0.02	0.03	0.35	0.04	0.02	0.02	0.01
LOI	7.91	10.93	5.34	10.50	10.20	10.20	3.61	4.51	8.90	3.55	3.57	13.10	10.58	11.70
	98.49	98.84	99.10	99.32	99.03	98.38	100.20	99.71	98.79	99.79	99.10	97.93	97.59	98.90

Cation proportions based on 100 cations

Si	43.70	39.80	44.30	39.05	40.66	40.84	47.71	44.50	39.54	44.95	47.79	38.77	39.08	37.97
Ti	0.15	0.10	0.09	0.07	0.09	0.09	0.13	0.15	0.21	0.37	0.26	0.18	0.13	0.05
Al	4.88	4.62	7.66	5.19	5.07	5.09	4.60	7.54	6.74	9.11	4.43	5.01	5.01	2.16
Mg	38.79	43.97	32.57	43.67	42.25	42.10	29.28	31.02	37.23	27.04	30.10	40.02	45.22	50.23
Fe	9.78	9.97	6.95	8.90	9.74	9.87	7.99	7.95	9.46	6.60	6.50	9.54	9.39	9.51
Mn	0.17	0.16	0.18	0.14	0.10	0.10	0.17	0.21	0.19	0.17	0.17	0.15	0.13	0.06
Ca	2.43	1.34	8.08	2.73	1.90	1.90	10.05	8.45	6.28	8.53	10.55	6.31	1.02	0.01
Na	0.09	0.02	0.18	0.23	0.19	0.0	0.05	0.16	0.30	0.78	0.15	0.0	0.0	0.0
K	0.0	0.0	0.0	0.0	0.0	0.0	0.0	0.01	0.03	2.18	0.01	0.0	0.0	0.0
P	0.02	0.02	0.01	0.02	0.01	0.01	0.02	0.02	0.02	0.28	0.03	0.02	0.02	0.01
O	146.27	142.22	148.13	141.63	143.20	143.49	150.14	148.35	142.99	148.81	150.23	141.48	141.75	139.12

Mg No	0.799	0.815	0.824	0.831	0.813	0.810	0.786	0.796	0.797	0.804	0.822	0.807	0.828	0.841
Al/Al+Si	0.100	0.104	0.147	0.117	0.111	0.111	0.088	0.145	0.146	0.168	0.085	0.115	0.114	0.054

Lagrande Yasinski

SAMPLE	84024 Perid	84026 Perid	84027 Pyrox	84029 Perid	84311 Perid	84312 Perid	84033 Pyrox	84050 Pyrox	84056 Perid	84114 Pyrox	41453 Pyrox	41454 Perid	41455 Perid	84166 Perid
Ni	711.	923.	1253.	1202.	914.	997.	300.	462.	892.	907.	1011.	1343.	1374.	1474.
Cr	3864.	2636.	1206.	1295.	2053.	2050.	1550.	3368.	2982.	1100.	4342.	6668.	8290.	1931.
V	115.	81.	90.	52.	72.	84.	77.	141.	119.	111.	98.	110.	98.	45.
Zr	—	—	—	—	—	—	—	—	—	85.	51.	45.	41.	—
Y	—	—	—	—	—	—	—	—	—	12.	12.	6.	6.	—
Nb	—	—	—	—	—	—	—	—	—	9.	9.	7.	9.	—
Rb	—	—	—	—	—	—	—	—	—	63.	13.	13.	14.	—
Sr	—	—	—	—	—	—	—	—	—	222.	8.	32.	12.	—
Ba	0.	0.	0.	0.	22.	0.	0.	0.	3.	154.	0.	40.	0.	0.

Lagrande Yasinski

SAMPLE	83068 Perid	84001 FineGb	84006 FineGb	84012 FineGb	84034 FineGb	84052 FineGb	84055 FineGb	84057 FineGb	84061 FineGb	84075 FineGb	84841 FineGb	84085 FineGb	84090 FineGb	84094 FineGb
SiO2	28.16	49.24	49.27	50.25	48.93	47.27	51.13	48.71	48.98	49.50	49.17	49.48	53.13	51.70
TiO2	0.02	1.29	1.00	0.99	0.82	1.62	1.04	1.42	1.33	0.60	0.92	0.96	0.79	0.92
Al2O3	0.58	13.55	14.11	14.04	15.00	13.54	13.74	13.81	14.12	15.55	13.82	15.20	14.35	14.47
MgO	36.47	5.51	7.32	6.62	7.04	6.23	6.74	5.83	6.53	8.03	6.74	6.37	6.68	6.57
FeO	12.70	15.47	12.88	12.89	11.15	15.68	11.43	14.95	14.34	10.79	13.28	11.68	8.38	11.49
MnO	0.19	0.26	0.23	0.21	0.21	0.23	0.20	0.24	0.23	0.20	0.20	0.21	0.19	0.20
CaO	0.05	9.67	10.74	10.51	11.21	9.68	10.68	9.41	8.69	9.93	9.48	11.28	8.67	8.56
Na2O	0.02	2.42	1.67	1.88	2.47	1.32	2.44	2.04	2.36	2.06	1.79	2.05	4.63	2.97
K2O	0.0	0.36	0.39	0.51	0.27	1.38	0.43	1.21	0.71	0.43	0.69	0.47	0.68	0.50
P2O5	0.0	0.10	0.09	0.08	0.06	0.11	0.08	0.13	0.13	0.05	0.08	0.07	0.51	0.08
LOI	21.28	1.54	2.08	1.47	1.85	2.09	1.71	1.65	2.58	1.44	3.39	2.26	1.64	2.16
	99.47	99.41	99.78	99.45	99.01	99.15	99.62	99.40	100.00	98.58	99.56	100.03	99.65	99.62

Cation proportions based on 100 cations

Si	29.93	47.74	47.45	48.32	46.86	46.42	48.85	47.23	47.35	47.29	48.18	47.45	49.50	49.40
Ti	0.02	0.94	0.72	0.72	0.59	1.20	0.75	1.04	0.97	0.43	0.68	0.69	0.55	0.66
Al	0.73	15.48	16.01	15.91	16.93	15.67	15.47	15.78	16.09	17.51	15.96	17.18	15.76	16.30
Mg	57.77	7.96	10.51	9.49	10.05	9.12	9.60	8.42	9.41	11.44	9.84	9.11	9.28	9.36
Fe	11.28	12.54	10.37	10.36	8.93	12.88	9.13	12.13	11.60	8.62	10.88	9.37	6.53	9.18
Mn	0.17	0.21	0.19	0.17	0.17	0.19	0.16	0.20	0.19	0.16	0.17	0.17	0.15	0.16
Ca	0.06	10.04	11.08	10.83	11.50	10.19	10.93	9.77	9.00	10.17	9.95	11.59	8.66	8.76
Na	0.04	4.55	3.12	3.51	4.59	2.51	4.52	3.83	4.42	3.82	3.40	3.81	8.36	5.50
K	0.0	0.45	0.48	0.63	0.33	1.73	0.52	1.50	0.88	0.52	0.86	0.57	0.81	0.61
P	0.0	0.08	0.07	0.07	0.05	0.09	0.06	0.11	0.11	0.04	0.07	0.06	0.40	0.06
O	130.29	154.05	154.49	155.03	153.53	153.47	154.91	153.64	153.87	154.37	154.81	154.63	153.95	155.25
Mg No.	0.837	0.388	0.503	0.478	0.530	0.415	0.512	0.410	0.448	0.570	0.475	0.493	0.587	0.505
Al/Al+Si	0.024	0.245	0.252	0.248	0.265	0.252	0.241	0.250	0.254	0.270	0.249	0.266	0.241	0.248

Lagrande Yasinski

SAMPLE	83068 Perid	84001 FineGb	84006 FineGb	84012 FineGb	84034 FineGb	84052 FineGb	84055 FineGb	84057 FineGb	84061 FineGb	84075 FineGb	84841 FineGb	84085 FineGb	84090 FineGb	84094 FineGb
Ni	1336.	34.	123.	103.	96.	92.	72.	70.	60.	103.	68.	66.	144.	102.
Cr	29.	63.	187.	169.	200.	110.	90.	126.	172.	238.	62.	185.	484.	217.
V	—	348.	295.	291.	262.	507.	280.	317.	331.	217.	311.	281.	171.	308.
Zr	35.	95.	—	—	—	—	—	107.	—	—	77.	—	—	72.
Y	2.	31.	—	—	—	—	—	34.	—	—	30.	—	—	26.
Nb	9.	9.	—	—	—	—	—	10.	—	—	8.	—	—	9.
Rb	14.	19.	—	—	—	—	—	58.	—	—	32.	—	—	23.
Sr	6.	136.	—	—	—	—	—	147.	—	—	149.	—	—	89.
Ba	—	64.	12.	120.	92.	208.	55.	175.	89.	53.	104.	66.	359.	79.

Lagrande Yasinski

SAMPLE	84103 FineGb	84110 FineGb	41451 FineGb	83108 FineGb	83131 FineGb	84030 CoarGb	84035 CoarGb	84071 CoarGb	84081 CoarGb	84083 CoarGb	84089 CoarGb	84095 CoarGb	84127 CoarGb	84128 CoarGb
SiO2	50.76	48.88	49.60	46.51	49.81	50.25	48.34	49.44	49.32	50.19	49.60	53.29	52.19	50.22
TiO2	1.16	1.54	0.93	2.26	0.77	0.17	0.25	0.34	0.47	0.28	0.19	0.48	0.67	0.30
Al2O3	13.27	13.97	14.13	12.99	14.75	15.76	15.25	14.64	14.62	15.25	14.98	14.14	14.55	13.21
MgO	5.20	5.68	6.91	5.20	8.34	12.36	13.07	12.63	7.32	10.42	12.23	7.07	5.90	10.55
FeO	15.13	15.18	12.98	17.40	10.90	6.49	7.86	7.82	11.73	6.32	6.19	11.50	11.65	7.96
MnO	0.28	0.24	0.25	0.26	0.20	0.15	0.17	0.16	0.20	0.15	0.15	0.19	0.24	0.18
CaO	9.98	9.23	9.52	10.02	11.16	8.09	9.29	9.46	8.47	12.79	12.06	6.89	10.51	14.66
Na2O	1.93	1.49	3.25	0.90	2.66	2.55	1.45	1.33	2.63	1.71	1.04	2.46	1.50	0.87
K2O	0.39	0.68	0.73	1.91	0.52	1.13	0.94	0.62	0.38	0.40	0.09	0.97	0.25	0.21
P2O5	0.11	0.14	0.08	0.18	0.05	0.02	0.02	0.03	0.04	0.03	0.02	0.09	0.05	0.03
LOI	1.09	2.61	0.80	1.44	0.99	3.90	3.46	3.75	2.61	2.53	3.35	2.61	2.21	1.94
	99.30	99.64	99.18	99.07	100.15	100.87	100.10	100.22	97.79	100.07	99.90	99.69	99.72	100.13

Cation proportions based on 100 cations

Si	49.31	48.10	46.87	46.00	46.42	46.53	45.31	46.65	48.12	46.96	46.79	51.19	50.61	47.27
Ti	0.85	1.14	0.66	1.68	0.54	0.12	0.18	0.24	0.34	0.20	0.13	0.35	0.49	0.21
Al	15.19	16.20	15.74	15.14	16.20	17.20	16.85	16.28	16.81	16.82	16.66	16.01	16.63	14.65
Mg	7.53	8.33	9.73	7.67	11.58	17.06	18.26	17.76	10.65	14.53	17.20	10.12	8.53	14.80
Fe	12.30	12.49	10.25	14.39	8.49	5.02	6.16	6.17	9.57	4.94	4.88	9.24	9.45	6.27
Mn	0.23	0.20	0.20	0.22	0.16	0.12	0.13	0.13	0.17	0.12	0.12	0.15	0.20	0.14
Ca	10.39	9.73	9.64	10.62	11.14	8.03	9.33	9.56	8.85	12.82	12.19	7.09	10.92	14.78
Na	3.64	2.84	5.96	1.73	4.81	4.58	2.64	2.43	4.98	3.10	1.90	4.58	2.82	1.59
K	0.48	0.85	0.88	2.41	0.62	1.33	1.12	0.75	0.47	0.48	0.11	1.19	0.31	0.25
P	0.09	0.12	0.06	0.15	0.04	0.02	0.02	0.02	0.03	0.02	0.02	0.07	0.04	0.02
O	155.83	155.66	152.08	153.41	152.41	152.31	152.06	153.48	154.20	153.82	154.27	156.77	157.91	153.93
Mg No.	0.380	0.400	0.487	0.348	0.577	0.772	0.748	0.742	0.526	0.746	0.779	0.523	0.474	0.702
Al/Al+Si	0.236	0.252	0.251	0.248	0.259	0.270	0.271	0.259	0.259	0.264	0.263	0.238	0.247	0.237

Lagrande Yasinski

SAMPLE	84103 FineGb	84110 FineGb	41451 FineGb ?	83108 FineGb	83131 FineGb	84030 CoarGb	84035 CoarGb	84071 CoarGb	84081 CoarGb	84083 CoarGb	84089 CoarGb	84095 CoarGb	84127 CoarGb	84128 CoarGb
Ni	19.	52.	136.	79.	157.	176.	217.	223.	60.	207.	215.	65.	32.	137.
Cr	63.	101.	230.	68.	342.	1275.	1279.	1135.	16.	558.	959.	29.	16.	89.
V	264.	357.	311.	—	—	98.	117.	138.	234.	162.	120.	238.	294.	174.
Zr	—	—	78.	128.	65.	—	42.	48.	—	—	—	74.	69.	46.
Y	—	—	27.	43.	18.	—	8.	9.	—	—	—	21.	16.	10.
Nb	—	—	8.	9.	8.	—	8.	8.	—	—	—	9.	9.	8.
Rb	—	—	34.	74.	26.	—	29.	27.	—	—	—	32.	18.	17.
Sr	—	—	168.	183	275.	—	105.	124.	—	—	—	100.	112.	67.
Ba	70.	133.	186.	—	—	278.	244.	101.	38.	43.	0.	181.	5.	8.

Lagrande Yasinski

SAMPLE	84130 CoarGb	84146 CoarGb	84148 CoarGb	84149 CoarGb	84150 CoarGb	84151 CoarGb	84154 CoarGb	83093 CoarGb	84011 ContGb	84078 ContGb	84842 ContGb	84087 ContGb	84096 ContGb	84098 ContGb
SiO2	50.11	48.78	49.89	49.01	52.24	50.41	50 57	48.63	55.47	55.02	58.25	58.25	56.13	59.40
TiO2	0.19	0.10	0.19	0.15	0.79	0.41	0.35	1.42	0.81	0.19	0.99	0.61	2.00	0.64
Al2O3	14.67	13.62	15.64	21.43	14.63	17.31	15.51	14.28	13.47	18.52	11.13	14.30	13.67	13.89
MgO	11.18	15.34	10.66	7.59	6.69	8.30	9.40	6.25	6.74	7.33	3.78	5.82	5.22	5.84
FeO	5.95	7.53	6.77	4.57	12.01	7.65	8.38	14.08	7.82	6.12	6.85	8.49	11.94	6.74
MnO	0.15	0.16	0.15	0.10	0.22	0.17	0.19	0.25	0 14	0.10	0.14	0.18	0.14	0.14
CaO	14.10	9.28	13.93	14.68	9.69	12.56	12.37	10.01	6.81	3.15	8.68	6.36	5.11	5.65
Na2O	0.99	1.28	0.91	1.42	2.25	1.46	1 72	2 12	3.33	2.62	3.12	2.63	1.02	4.02
K2O	0.34	0.16	0 07	0.08	0.17	0.28	0.12	0 49	2.90	3.50	0.28	0.78	0.59	1.52
P2O5	0.02	0.01	0.02	0.02	0.09	0.04	0 03	0.11	0 27	0.03	0.14	0.07	0.84	0.34
LOI	1.98	3.85	1.23	0 79	0.68	1.25	0.65	1.71	2 00	1.72	6 75	2.66	3.62	1.58
	99.68	100.11	99.46	99.84	99.46	99.84	99.29	99 35	99 76	98.30	100.11	100.15	100.28	99.76

Cation proportions based on 100 cations

Si	46.93	45.66	46.65	45.30	49.60	47.24	47.24	47.04	52.16	51.88	58.59	55.76	55.83	55.63
Ti	0 13	0.07	0.13	0.10	0.56	0.29	0 25	1.03	0.57	0 13	0.75	0.44	1.50	0.45
Al	16.19	15.02	17.24	23.34	16.37	19.12	17.07	16.28	14.93	20.58	13.19	16.13	16.02	15.33
Mg	15.61	21 40	14.86	10.46	9.47	11.59	13 09	9 01	9.45	10 30	5.67	8.30	7.74	8.15
Fe	4.66	5.90	5.29	3.53	9 54	5.99	6 54	11.39	6.15	4.82	5.76	6 80	9.93	5.28
Mn	0.12	0 13	0.12	0.08	0.18	0.13	0.15	0.20	0 11	0.08	0.12	0.15	0.12	0.11
Ca	14 15	9.31	13.96	14.54	9.86	12.61	12.38	10.37	6.86	3 18	9.35	6.52	5.45	5.67
Na	1.80	2.32	1.65	2.54	4.14	2.65	3 12	3 98	6 07	4.79	6.08	4.88	1.97	7.30
K	0.41	0.19	0.08	0.09	0.21	0.33	0.14	0.60	3 48	4 21	0.36	0.95	0.75	1.82
P	0.02	0.01	0.02	0.02	0.07	0.03	0.02	0.09	0.21	0.02	0.12	0.06	0.71	0.27
O	154.08	151.99	154.56	155 78	156.29	155.64	154.43	154.05	155 75	157.84	162.90	161.44	165.04	159.59
Mg No.	0.770	0.784	0.737	0.747	0.498	0.659	0.667	0.442	0.606	0.681	0.496	0.550	0.438	0.607
Al/Al+Si	0.257	0.248	0.270	0.340	0.248	0.288	0.266	0.257	0.223	0 284	0.184	0 224	0.223	0.216

Lagrande Yasinski

SAMPLE	84130 CoarGb	84146 CoarGb	84148 CoarGb	84149 CoarGb	84150 CoarGb	84151 CoarGb	84154 CoarGb	83093 CoarGb	84011 ContGb	84078 ContGb	84842 ContGb	84087 ContGb	84096 ContGb	84098 ContGb
Ni	184.	509.	141.	104.	58.	103.	140.	79.	74.	49.	36.	55.	134.	105.
Cr	388.	1222.	896.	737	27.	605.	703.	205.	387.	53.	14.	141.	10.	361.
V	129.	96.	152.	105.	291.	174.	157.	—	162.	85.	234.	177.	37.	120.
Zr	40.	34.	—	—	—	—	48	102	116.	62.	—	85.	118.	134.
Y	7.	4.	—	—	—	—	12.	34	16.	4.	—	18.	45.	19.
Nb	8.	8.	—	—	—	—	8.	10.	8.	8.	—	9.	11.	11.
Rb	22.	20.	—	—	—	—	15.	23.	111.	81.	—	29.	25.	37.
Sr	63.	58.	—	—	—	—	80.	157.	569.	74.	—	263.	65.	431.
Ba	17.	0.	22.	21.	0.	36.	34.	—	710.	550.	76.	241.	104.	408.

Lagrande-Yasinski

SAMPLE	83117 ContGb	84159 LTiLav	84161 LTiLav	84162 LTiLav	84163 LTiLav	20007 LTiLav	20012 LTiLav	20013 LTiLav	20014 LTiLav	83151 LTiLav	84157 ITiLav	84158 ITiLav	84160 ITiLav	20001 ITiLav
SiO2	52.62	48.67	52.86	52.80	51.70	53.58	50.21	51.44	51.49	55.79	48.60	47.58	53.74	49.70
TiO2	0.82	0.47	0.66	0.74	0.71	0.74	0.83	0.68	0.69	0.68	0.89	0.86	0.95	1.00
Al2O3	14.03	16.51	15.21	13.73	14.91	11.74	14.96	16.41	16.41	13.39	15.50	16.04	14.35	15.45
MgO	7.76	8.81	7.15	5.43	8.29	10.82	8.18	5.42	4.42	5.66	7.02	8.51	6.81	6.05
FeO	8.59	8.91	8.77	10.21	9.07	8.36	10.22	8.58	8.75	10.17	11.95	11.81	10.33	9.96
MnO	0.16	0.18	0.23	0.30	0.21	0.16	0.20	0.18	0.18	0.25	0.22	0.22	0.31	0.19
CaO	9.13	13.36	11.91	12.11	10.73	9.66	12.34	13.55	14.67	10.82	12.53	11.19	8.03	13.43
Na2O	3.99	1.53	1.59	1.90	3.05	2.24	1.86	1.96	1.50	1.72	2.01	2.24	4.07	1.88
K2O	1.13	0.21	0.09	0.18	0.15	0.87	0.27	0.45	0.12	0.20	0.18	0.24	0.24	0.11
P2O5	0.38	0.03	0.06	0.05	0.05	0.44	0.04	0.05	0.05	0.04	0.08	0.07	0.09	0.07
LOI	1.20	0.74	0.87	2.66	0.70	1.17	0.97	1.07	1.53	1.59	0.53	1.00	0.39	2.33
	99.81	99.42	99.40	100.11	99.57	99.78	99.88	99.79	99.81	100.31	99.51	99.76	99.31	100.17

Cation proportions based on 100 cations

Si	48.75	45.59	50.11	51.08	48.06	49.89	47.18	48.70	49.40	53.41	45.94	44.65	50.09	47.60
Ti	0.57	0.33	0.47	0.54	0.50	0.52	0.45	0.48	0.50	0.49	0.63	0.61	0.67	0.72
Al	15.32	18.22	16.99	15.66	16.34	12.88	16.57	18.31	18.56	15.11	17.27	17.74	15.76	17.44
Mg	10.72	12.30	10.10	7.83	11.49	15.02	11.46	7.65	6.32	8.08	9.89	11.90	9.46	8.64
Fe	6.66	6.98	6.96	8.26	7.05	6.51	8.03	6.80	7.02	8.14	9.45	9.26	8.05	7.98
Mn	0.13	0.14	0.18	0.25	0.17	0.13	0.16	0.14	0.15	0.20	0.18	0.17	0.24	0.15
Ca	9.06	13.40	12.10	12.55	10.69	9.64	12.42	13.74	15.08	11.10	12.69	11.25	8.02	13.78
Na	7.17	2.78	2.92	3.56	5.50	4.04	3.39	3.60	2.79	3.19	3.68	4.08	7.35	3.49
K	1.34	0.25	0.11	0.22	0.18	1.03	0.32	0.54	0.15	0.24	0.22	0.29	0.29	0.13
P	0.30	0.02	0.05	0.04	0.04	0.35	0.03	0.04	0.04	0.03	0.06	0.06	0.07	0.06
O	153.18	153.54	157.64	157.62	153.95	154.83	154.10	156.32	157.77	159.79	153.35	152.02	154.92	155.32
Mg No.	0.617	0.638	0.592	0.487	0.620	0.698	0.588	0.529	0.474	0.498	0.511	0.562	0.540	0.520
Al/Al+Si	0.239	0.286	0.253	0.235	0.254	0.205	0.260	0.273	0.273	0.220	0.273	0.284	0.239	0.268

Lagrande, Yasinski

SAMPLE	83117 ContGb	84159 LTiLav	84161 LTiLav	84162 LTiLav	84163 LTiLav	20007 LTiLav	20012 LTiLav	20013 LTiLav	20014 LTiLav	83151 LTiLav	84157 ITiLav	84158 ITiLav	84160 ITiLav	20001 ITiLav
Ni	79.	183.	99.	111.	153.	232.	159.	121.	151.	157.	122.	136.	68.	126.
Cr	410.	429.	312.	815.	361.	794.	397.	407.	431.	821.	304.	298.	227.	328.
V	—	183.	264.	247.	246.	145	225.	257.	267.	—	263.	273.	254.	299.
Zr	105.	53.	62.	73.	65.	—	60.	62.	63.	69.	79.	74.	87.	81.
Y	18.	13.	17.	18.	19.	—	17.	18.	21.	18.	26.	24.	23.	25.
Nb	11.	8.	8	10	8.	—	8.	9.	9.	10.	9.	8.	9.	9.
Rb	40.	18.	14.	13.	14.	—	18	25.	14.	15.	15.	17.	15.	15.
Sr	570.	161.	113	95.	107.	—	78.	118.	144.	83.	112.	125.	98.	182.
Ba	—	11.	33.	43.	27.	365.	54.	52.	0:	—	30.	43.	37.	69.

Lagrande Yasinski

SAMPLE	20002 ITiLav	20004 ITiLav	20005 ITiLav	20006 ITiLav	20008 ITiLav	20009 ITiLav	20010 ITiLav	20011 ITiLav	83152 ITiLav	83153 ITiLav	84164 HTiLav	84165 HTiLav	83150 HTiLav	83145 HTiLav
SiO2	49.76	50.01	49.83	50.23	51.03	49.22	50.66	50.22	48.67	48.55	50.86	50.75	49.05	47.90
TiO2	0.95	0.98	0.97	0 97	0.96	0.96	1.02	0.92	0.92	0.87	1.31	1 32	1.38	1.42
Al2O3	15.30	15.03	15.50	15.13	15.40	15 55	16 44	15.20	15.85	15.70	11.09	11.08	11.46	15.41
MgO	7.05	7.38	7.32	5.12	7.02	7.20	4 65	6.99	6.86	6.31	6.78	7.09	6.80	7.15
FeO	11.59	11.49	11.81	9.61	11.40	11.39	9.08	12.29	11 78	11.31	11.37	10.93	11.29	11.97
MnO	0.18	0.20	0.18	0.18	0.17	0 18	0.17	0.22	0.22	0.23	0.21	0.20	0.23	0.16
CaO	11.59	11.39	11.05	13.41	10.50	11.98	12 83	10.04	11.63	13.27	12.52	12.00	13.69	9.66
Na2O	1.94	2.23	2.11	2.11	2 49	2.12	2.59	2 63	2 70	1.85	2.37	2.07	2.55	3.04
K2O	0 08	0.14	0.15	0.12	0.19	0.15	0.21	0.42	0.25	0.21	0.31	0.84	0.44	1.00
P2O5	0.07	0.07	0.07	0.06	0.06	0.07	0.07	0.08	0.06	0.06	0.10	0.10	0.10	0.18
LOI	0.79	0.92	0.58	2.85	1.17	0.60	2.47	0 49	0.69	1.40	2.44	2.40	3.43	2.87
	99.30	99.84	99.57	99.79	100.39	99.42	100.19	99.50	99.63	99.76	99.36	98.78	100.42	100.76

Cation proportions based on 100 cations

Si	47 30	47.18	47.03	48.64	47 95	46 49	48 45	47.30	45 76	46.29	49.28	49 41	47.33	45.36
Ti	0.68	0 70	0.69	0.71	0 68	0.68	0 73	0 65	0.65	0 62	0.95	0.97	1.00	1.01
Al	17.14	16.71	17.24	17.27	17.06	17.31	18 53	16.87	17.56	17.64	12.67	12 71	13.03	17.20
Mg	9.99	10 38	10.30	7.39	9.83	10.14	6.63	9.81	9.61	8.97	8.79	10.29	9.78	10.09
Fe	9 21	9.07	9.32	7.78	8.96	9.00	7.26	9.68	9.26	9.02	9.22	8.90	9.11	9.48
Mn	0.14	0.16	0.14	0.15	0.14	0.14	0 14	0.18	0 18	0.19	0.17	0.16	0.19	0.13
Ca	11.80	11 51	11 17	13 91	10.57	12 12	13.15	10 13	11 71	13 55	13.00	12.52	14.15	9.80
Na	3.58	4 08	3.86	3.96	4.54	3.88	4.80	4.80	4 92	3.42	4 45	3.91	4.77	5.58
K	0.10	0.17	0.18	0.15	0.23	0.18	0.26	0.50	0.30	0 26	0 38	1.04	0.54	1.21
P	0.06	0 06	0.06	0.05	0.05	0.06	0 06	0.06	0.05	0.05	0.08	0.08	0.08	0.14
O	154 80	154 19	154.41	156.00	154 85	153.88	156.00	153 83	152 65	153 97	154 28	154.38	152.32	151.79
Mg No	0.520	0.534	0.525	0.487	0.523	0.530	0.477	0 503	0 509	0.499	0.515	0.536	0.518	0.516
Al/Al+Si	0.266	0 262	0 268	0 262	0 262	0 271	0 277	0.263	0.277	0.276	0.204	0.205	0.216	0.275

Lagrande Yasinski

SAMPLE	20002 ITiLav	20004 ITiLav	20005 ITiLav	20006 ITiLav	20008 ITiLav	20009 ITiLav	20010 ITiLav	20011 ITiLav	83152 ITiLav	83153 ITiLav	84164 HTiLav	84165 HTiLav	83150 HTiLav	83145 HTiLav
Ni	126.	121.	136.	133.	154.	130.	236.	140	79.	79.	156.	150.	79.	79.
Cr	315.	317.	307.	334.	334.	317.	446.	203.	205.	274.	297.	283.	274.	68.
V	289.	269.	293	280.	287.	275.	281	296.	—	—	249.	239.	—	—
Zr	78.	80	78.	80.	79.	78.	78	79	74.	74.	—	120.	118.	107.
Y	24.	24	25.	25	26.	25.	25.	24.	23.	24.	—	21.	22.	25.
Nb	9.	9.	8	9	9.	9.	9.	9.	9.	9.	—	22.	20.	11.
Rb	14.	14.	14.	14.	15.	14.	16.	20.	14.	15.	—	28.	19.	42.
Sr	113.	139.	147.	149.	178.	143.	229	235.	97.	105.	—	283.	624.	225.
Ba	1.	35.	32.	27.	49.	29.	66.	42.	—	—	68.	175.	—	—

Lagrande Vastinskt

SAMPLE	84005 Tonal	84010 Tonal	84014 Tonal	84021 Tonal	84051 Tonal	84054 Tonal	84058 Tonal	84059 Tonal	84063 Tonal	84064 Tonal	84072 Tonal	84074 Tonal	84079 Tonal	84086 Tonal
SiO2	72.79	71.55	70 44	72.14	69.90	69.71	71.46	70.35	71 14	69.55	71.14	71.27	70.69	67.67
TiO2	0.17	0.26	0.37	0.25	0 20	0.25	0.25	0.24	0 27	0.30	0.28	0.23	0.24	0.35
Al2O3	14.87	15.57	14.85	15.22	16.22	16.18	15.48	14.59	15.26	14.52	14 32	14.36	14.89	13.64
MgO	0.43	0.55	0 75	1.07	1.60	1.54	0.74	1.51	0.94	1.83	1 73	1.22	1.98	4.31
FeO	1 12	1.89	3 24	1.84	1 47	1.72	1.47	1.91	1.94	2.53	2 56	2 49	2.86	5.68
MnO	0 03	0.02	0.06	0.03	0.04	0.04	0.02	0.05	0 03	0.05	0.05	0 04	0.07	0.14
CaO	1.64	2 73	2 97	1 10	2 19	1 93	2 44	2.61	1 71	2 50	2 10	2.49	1.32	0.73
Na2O	5.29	5.20	4.04	7 26	1 48	0.89	4 48	0.68	4.80	1 97	2 92	4.20	3.35	4.35
K2O	1 95	1.30	2.08	0 52	4.03	4 66	1 89	4 39	1 89	3 08	2.57	1.77	2.39	0.69
P2O5	0.07	0.09	0.09	0 10	0 05	0.07	0.09	0.08	0 09	0.09	0 09	0 04	0.08	0.06
LOI	1 73	1 07	1.30	0.55	3.60	3.23	1 92	4.03	2.04	3 82	2.24	1.49	2.80	2.50
	100.09	100 23	100.19	100.08	100.78	100.22	100 24	100.44	100 11	100 24	100.00	99.60	100.17	100.12

Cation proportions based on 100 cations

Si	68 28	66 71	66.55	65.93	67 73	67 99	67.40	69.38	67 11	68.00	68.23	67.61	67.69	64.17
Ti	0.12	0.18	0 26	0.17	0.15	0.18	0 18	0.18	0.19	0.22	0.20	0.16	0.17	0.25
Al	16.44	17.11	16.54	16.39	18.52	18.60	17 21	16.96	16 97	16 73	16.19	16.06	16.81	15.25
Mg	0.60	0.76	1.06	1.46	2.31	2.24	1.04	2 22	1.32	2.67	2.47	1.73	2.83	6.09
Fe	0 88	1.47	2.56	1 40	1.19	1.40	1 16	1.57	1.53	2 07	2.06	1.98	1.89	4.50
Mn	0.02	0 02	0.05	0 02	0.03	0.03	0.02	0.04	0 02	0 04	0.04	0.03	0.06	0.11
Ca	1 65	2 73	3 01	1.08	2.27	2.02	2.47	2 76	1 73	2 62	2.16	2.53	1.35	0.74
Na	9.62	9.40	7 40	12 86	2 78	1.68	8 19	1 30	8.78	3 73	5 43	7.73	6 22	8.00
K	2.33	1.55	2.51	0 61	4.98	5.80	2 27	5 52	2 27	3.84	3 14	2.14	2.92	0.83
P	0.06	0 07	0 07	0 08	0.04	0.06	0 07	0.07	0 07	0.07	0 07	0.03	0 06	0.05
O	170.72	170.08	170 24	167.68	173 31	173.82	171 05	174.73	170.37	172 91	172.35	170.92	171.80	167.70
Mg No.	0 405	0 342	0 292	0 510	0 660	0 615	0.473	0 585	0 463	0 563	0 546	0 466	0 600	0.575
Al/Al+Si	0.194	0 204	0 199	0 199	0.215	0.215	0 203	0 196	0 202	0 197	0 192	0.192	0.199	0.192

Lagrande Yasinski

SAMPLE	84005	84010	84014	84021	84051	84054	84058	84059	84063	84064	84072	84074	84079	84086
	Tonal	Tonal	Tonal	Tonal	Tonal	Tonal	Tonal	Tonal	Tonal	Tonal	Tonal	Tonal	Tonal	Tonal
Ni	36.	7.	19.	13.	51.	21.	13.	12.	9.	13.	5.	28.	18.	43.
Cr	0.	7.	12.	0	45.	1.	12	7.	0	10	0.	12.	0.	38.
V	6.	12	32.	20.	22.	15.	10.	2	32.	18.	24.	48.	4.	73.
Zr	136	—	—	142.	—	—	—	132.	135.	160.	160.	124.	124.	107.
Y	5	—	—	11.	—	—	—	5.	7	6.	7.	11.	5.	9.
Nb	6.	—	—	10.	—	—	—	10.	9.	9.	10.	9.	11.	11.
Rb	62	—	—	27.	—	—	—	127	63.	91.	62.	50.	63.	23.
Sr	258.	—	—	154.	—	—	—	41.	142	59.	113.	103.	40.	129.
Ba	676.	221.	502.	243.	481.	495.	208.	509	182	246	586.	494.	119.	155.

Lagrande Yasinski

SAMPLE	84088 Tonal	84099 Tonal	84101 Tonal	84109 Tonal	84137 Tonal	84138 Tonal	84139 Tonal	84140 Tonal
SiO2	72.36	66 90	66 95	71.56	72.70	74.90	70.95	72.19
TiO2	0.21	0.32	0.48	0 22	0.23	0.15	0 29	0.33
Al2O3	15.60	13.54	14.03	15.19	15.14	14.40	16.01	14.21
MgO	0.72	4 99	2.08	0 53	0.47	0.25	0.50	0.50
FeO	1.54	6.09	5.73	1.65	1.63	1.06	1.57	2.65
MnO	0.04	0.13	0.06	0 02	0 02	0.01	0.01	0.05
CaO	1.65	1.52	4.12	1 70	2.28	1.45	1 45	2.14
Na2O	5.67	1 27	3 80	5 29	5.36	5.78	5 96	4.05
K2O	1.34	2 02	1.28	1.89	1.12	1.20	1 73	2 92
P2O5	0.07	0.05	0.07	0.07	0 07	0.05	0 10	0.08
LOI	1.14	3 46	1.52	1.95	0.99	0.73	1 66	0.80
	100.34	100 29	100.12	100.07	100.01	99.97	100.23	99.92

Cation proportions based on 100 cations

Si	67.11	65 30	63.60	67 28	67.87	69 62	66 00	68.02
Ti	0.15	0.23	0 34	0 16	0.16	0.10	0 20	0.23
Al	17.05	15 58	15.71	16.83	16.66	15.78	17.55	15.78
Mg	1.00	7.26	2 95	0 74	0.65	0.35	0.69	0.70
Fe	1.19	4 97	4.55	1 29	1 27	0.82	1 22	2.08
Mn	0.03	0.11	0 05	0.02	0 02	0 01	0.01	0.04
Ca	1.64	1.59	4.19	1.71	2 28	1.44	1 45	2.16
Na	10.20	2 40	7.00	9.64	9 70	10.42	10 75	7.40
K	1.59	2.52	1 55	2.27	1 33	1.42	2.05	3.51
P	0.05	0.04	0.06	0.06	0.06	0.04	0.08	0.06
O	169 97	170 93	167.61	169.98	170 92	171.76	168 70	170.79

Mg Mg	0.455	0 593	0.393	0.365	0 340	0 297	0 363	0 252
Al/Al+Si	0.203	0.193	0 198	0 200	0 197	0 185	0.210	0.188

Lagrande Yasinski

SAMPLE	84088 Tonal	84099 Tonal	84101 Tonal	84109 Tonal	84137 Tonal	84138 Tonal	84139 Tonal	84140 Tonal
Ni	17.	35	36.	9.	11.	17.	11.	18.
Cr	0	99.	32.	6.	7.	8.	3.	0.
V	16	88	109	18	14	8	26.	26.
Zr	—	99.	128.	—	139.	121.	—	166.
Y	—	13.	21	—	6.	9.	—	29.
Nb	—	11.	12	—	9.	8.	—	12
Rb	—	52.	59.	—	37	38.	—	95.
Sr	—	78.	155	—	351.	217.	—	127.
Ba	202.	193.	282.	456.	250.	454.	431.	621.

Lagrande Vasinski

SAMPLE	83059 Perid	83021 Perid	83022 Perid	83048 Perid	83058 Perid	83069 Perid	83074 Perid	83075 Perid	83077 Perid	83088 Perid	83089 Perid	83092 Perid	83094 Perid	83097 Perid
SiO2	34.71	27.20	31.55	41.11	35.30	32.32	36.60	36.95	33.93	36.21	39.08	36.79	38.32	40.32
TiO2	0.03	0.02	0.04	0.09	0.02	0.01	0.03	0.04	0.04	0.06	0.09	0.08	0.10	0.09
Al2O3	0.73	0.69	0.80	3.30	1.23	0.62	0.96	1.35	1.19	1.97	2.73	2.85	3.83	2.94
MgO	37.56	34.54	35.19	33.92	36.01	35.25	36.70	35.79	36.39	35.38	34.46	32.61	33.59	33.41
FeO	9.62	10.43	11.30	9.61	9.50	14.31	9.25	11.30	10.92	10.51	10.66	11.11	10.01	10.92
MnO	0.16	0.20	0.19	0.15	0.14	0.13	0.20	0.12	0.13	0.19	0.13	0.14	0.15	0.15
CaO	0.01	3.01	0.21	0.22	0.02	0.01	0.02	0.0	0.0	0.46	0.34	1.10	1.49	0.02
Na2O	0.04	0.0	0.04	0.05	0.07	0.07	0.04	0.0	0.0	0.05	0.02	0.0	0.04	0.0
K2O	0.0	0.01	0.0	0.01	0.0	0.0	0.0	0.01	0.0	0.0	0.0	0.0	0.01	0.0
P2O5	0.01	0.01	0.01	0.01	0.0	0.0	0.0	0.01	0.0	0.01	0.0	0.0	0.01	0.0
LOI	16.99	22.03	19.71	10.19	16.97	15.90	15.20	13.18	16.18	13.81	10.92	13.73	12.04	10.58
	99.86	98.14	99.04	98.66	99.26	98.62	99.00	98.75	98.78	98.65	98.43	98.41	99.59	98.43

Cation proportions based on 100 cations

Si	34.76	29.68	33.25	39.47	35.78	33.04	36.43	36.41	34.33	35.90	37.88	37.01	37.14	39.17
Ti	0.02	0.02	0.03	0.06	0.02	0.01	0.02	0.03	0.03	0.04	0.07	0.06	0.07	0.07
Al	0.86	0.89	0.99	3.73	1.47	0.75	1.13	1.57	1.42	2.30	3.12	3.38	4.38	3.37
Mg	56.07	56.17	55.27	48.55	54.40	53.71	54.45	52.56	54.87	52.29	49.79	48.90	48.53	48.38
Fe	8.06	9.52	9.96	7.72	8.05	12.23	7.70	9.31	9.24	8.71	8.64	9.35	8.11	8.87
Mn	0.14	0.18	0.17	0.12	0.12	0.11	0.17	0.10	0.11	0.16	0.11	0.12	0.12	0.12
Ca	0.01	3.52	0.24	0.23	0.02	0.01	0.02	0.0	0.0	0.49	0.35	1.19	1.55	0.02
Na	0.08	0.0	0.08	0.09	0.14	0.14	0.08	0.0	0.0	0.10	0.04	0.0	0.08	0.0
K	0.0	0.01	0.0	0.01	0.0	0.0	0.0	0.01	0.0	0.0	0.0	0.0	0.01	0.0
P	0.01	0.01	0.01	0.01	0.0	0.0	0.0	0.01	0.0	0.01	0.0	0.0	0.01	0.0
O	135.19	130.15	133.75	141.37	136.46	133.35	136.98	137.23	135.07	137.06	139.49	138.76	139.37	140.92
Mg No.	0.874	0.855	0.847	0.863	0.871	0.815	0.876	0.849	0.856	0.857	0.852	0.839	0.857	0.845
Al/Al+Si	0.024	0.029	0.029	0.086	0.039	0.022	0.030	0.041	0.040	0.060	0.076	0.084	0.105	0.079

Lagrande Yasinski

SAMPLE	83059 Perid	88021 Perid	83022 Perid	83048 Perid	83058 Perid	83069 Perid	83074 Perid	83075 Perid	83077 Perid	83088 Perid	83089 Perid	83092 Perid	83094 Perid	83097 Perid
Ni	864.	2672.	1414.	1414.	1100.	1021.	1414.	990.	1414.	1257.	1336.	1257.	1336.	1179.
Cr	2531.	2121.	3284.	5816.	2874.	6158.	2668.	5337.	5200.	3489.	6158.	6295.	684.	5063.

Lagrande Yasinski

SAMPLE	83104 Perid	83110 Perid	83119 Perid	83121 Perid	83046 FineGb	83065 FineGb	83083 FineGb	83084 FineGb	83102 FineGb	83109 FineGb	83111 FineGb	83120 FineGb	83123 FineGb	83130 FineGb
SiO2	38.54	37.07	39.95	38.65	49.62	49.18	51.78	48.81	49 34	49.79	48.36	48.68	53.99	49.94
TiO2	0.11	0.13	0.16	0.11	0.98	0 90	0.74	0.89	0.92	1 82	0 65	1.02	1.56	1.45
Al2O3	3.47	3.46	4.96	3.54	14.25	14.90	13.34	14.97	14.54	14 32	15.87	13.54	14.22	14.36
MgO	32.93	32.39	29.61	33.40	7.99	8.04	8.67	8.30	7.34	4.55	9.01	7.97	3.96	6.32
FeO	11.35	11.55	11.02	10.47	12.62	11.54	8.89	11.06	12.10	14 63	10.36	11 63	11.95	13.45
MnO	0.18	0.19	0.18	0.16	0.21	0.20	0.18	0.21	0 21	0.24	0.21	0.22	0.17	0.23
CaO	1.21	1.73	3.43	1.57	8.96	10.97	8.18	10.57	11.24	8.83	10.34	11.84	8 21	9.29
Na2O	0.06	0.07	0.06	0.07	2.62	1.80	3.15	2.20	1.11	2 82	2 02	2.54	3.79	3.04
K2O	0.01	0.0	0.01	0.01	1.15	0.50	2.39	0.84	0.37	0.51	0.91	0 62	1.03	0.75
P2O5	0.01	0.0	0.01	0.01	0.07	0.06	0.31	0.05	0.05	0.20	0 04	0 06	0.14	0.13
LOI	10.87	11.69	9.66	10.89	1.18	1.17	2.33	1.92	2.48	1.66	1.62	1.64	0.56	0.77
	98.74	98.28	99.05	98.88	99.65	99.26	99.96	99.82	99 70	99.37	99.39	99 76	99.58	99.73

Cation proportions based on 100 cations

Si	37.46	36.58	38.70	37.37	46.81	46 77	48.51	46.21	47 85	48.34	45.62	46.08	51.16	47.23
Ti	0.08	0.10	0 12	0 08	0.70	0.64	0 52	0 63	0.67	1 33	0.46	0.73	1.11	1.03
Al	3.98	4.02	5.66	4.03	15 84	16.70	14.73	16.70	16.62	16.38	17 64	15.11	15.88	16.01
Mg	47.71	47.64	42 75	48.14	11.24	11.40	12 11	11 71	10 61	6.58	12.67	11.24	5.59	8.91
Fe	9.22	9.53	8.93	8.47	9.95	9 17	6.96	8.76	9.82	11.88	8.17	9.20	9.47	10.64
Mn	0.15	0.16	0 15	0.13	0.17	0.16	0 14	0.17	0.17	0.20	0.17	0.18	0.14	0.18
Ca	1.26	1.83	3.56	1.63	9.06	11.18	8.21	10.72	11.68	9.18	10.45	12 01	8.33	9.41
Na	0.11	0.13	0.11	0 13	4.79	3.32	5 72	4.04	2 09	5 31	3.69	4.66	6.96	5.57
K	0.01	0.0	0.01	0.01	1.38	0.61	2 86	1.01	0.46	0.63	1.10	0.75	1.24	0.90
P	0.01	0.0	0.01	0.01	0.06	0.05	0.25	0.04	0.04	0.16	0.03	0.05	0.11	0.10
O	139.48	138.62	141.60	139.41	152.43	153 88	152 47	152.73	155 62	155.14	152 55	151 72	156.27	153.18
Mg No.	0.838	0.833	0.827	0.850	0.530	0.554	0 635	0.572	0.519	0.357	0.608	0 550	0.371	0.456
Al/Al+Si	0.096	0.099	0.128	0.097	0.253	0.263	0 233	0.265	0 258	0.253	0.279	0.247	0.237	0.253

Lagrande Yasinski

SAMPLE	83104	83110	83119	83121	83046	83065	83083	83084	83102	83109	83111	83120	83123	83130
	Perid	Perid	Perid	Perid	FineGb	FineGb	FineGb	FineGb	FineGb	FineGb	FineGb	FineGb	FineGb	FineGb
Ni	1021.	1336.	943.	1179.	79.	79.	79.	79.	79.	79.	157.	79.	79.	79.
Cr	4858.	342.	3695.	4995.	205.	65.	479.	342.	205.	68.	342.	274.	68.	137.

Lagrande Yasinski

SAMPLE	83112 FineGb	83132 FineGb	83133 FineGb	83041 CoarGb	83043 CoarGb	83044 CoarGb	83045 CoarGb	83049 CoarGb	83050 CoarGb	83051 CoarGb	83053 CoarGb	83090 CoarGb	83095 CoarGb	83098 CoarGb
SiO2	48.89	49.28	47.61	49.31	48.51	52.83	51.52	49.24	49.20	49.79	50.37	48.06	51.14	47.57
TiO2	1.56	0.98	0.99	0.29	0.42	0.38	0.50	0.28	0.61	0.34	0.12	0.20	0.58	0.96
Al2O3	13.60	15.15	14.63	15.70	13.34	14.16	14.43	15.71	14.19	16.22	14.59	14.81	14.36	15.43
MgO	5.94	7.75	8.52	9.98	9.64	8.74	8.09	9.92	9.58	11.05	13.32	11.09	9.00	8.12
FeO	15.76	12.03	12.53	7.68	9.50	7.08	7.70	7.67	10.40	7.57	6.29	10.00	9.34	14.03
MnO	0.27	0.20	0.21	0.13	0.20	0.14	0.14	0.14	0.19	0.15	0.15	0.22	0.18	0.25
CaO	7.64	10.15	11.40	12.76	14.54	9.54	12.86	12.87	11.28	9.88	10.61	8.57	10.82	7.17
Na2O	2.44	2.23	1.69	2.02	1.38	3.65	2.62	2.07	1.99	2.77	1.88	2.07	1.64	2.67
K2O	0.84	1.22	1.09	0.60	0.13	1.31	0.52	0.56	0.79	0.31	1.27	2.70	0.71	0.93
P2O5	0.12	0.07	0.03	0.01	0.04	0.01	0.03	0.01	0.02	0.02	0.01	0.01	0.05	0.07
LOI	2.20	1.16	1.25	1.76	2.32	2.51	1.99	1.45	1.46	2.36	2.47	2.61	2.16	3.15
	99.26	100.22	99.95	100.24	100.02	100.35	100.40	99.92	99.71	100.46	101.08	100.34	99.98	100.35

Cation proportions based on 100 cations

Si	47.73	46.29	44.98	45.74	45.99	48.98	48.12	45.67	46.20	45.91	45.98	44.75	48.43	45.47
Ti	1.15	0.69	0.70	0.20	0.30	0.26	0.35	0.20	0.43	0.24	0.08	0.14	0.41	0.69
Al	15.65	16.77	16.29	17.17	14.90	15.47	15.88	17.17	15.70	17.63	15.70	16.25	16.03	17.38
Mg	8.64	10.85	12.00	13.80	13.62	12.08	11.26	13.72	13.41	15.19	18.12	15.39	12.70	11.57
Fe	12.86	9.45	9.90	5.95	7.53	5.49	6.02	5.95	8.17	5.84	4.80	7.78	7.40	11.21
Mn	0.22	0.16	0.17	0.10	0.16	0.11	0.11	0.11	0.15	0.12	0.12	0.17	0.14	0.20
Ca	7.99	10.21	11.54	12.68	14.77	9.48	12.87	12.79	11.35	9.76	10.38	8.55	10.98	7.34
Na	4.62	4.06	3.10	3.63	2.54	6.56	4.74	3.72	3.62	4.95	3.33	3.74	3.01	4.95
K	1.05	1.46	1.31	0.71	0.16	1.55	0.62	0.66	0.95	0.36	1.48	3.21	0.86	1.13
P	0.10	0.06	0.02	0.01	0.03	0.01	0.02	0.01	0.02	0.02	0.01	0.01	0.04	0.06
O	154.01	152.69	151.66	152.37	152.44	152.94	153.77	152.28	152.22	152.32	151.52	149.56	154.98	151.89
Mg No.	0.402	0.534	0.548	0.699	0.644	0.687	0.652	0.698	0.621	0.722	0.791	0.664	0.632	0.508
Al/Al+Si	0.247	0.266	0.266	0.273	0.245	0.240	0.248	0.273	0.254	0.277	0.255	0.266	0.249	0.277

Layrande Yasinski

SAMPLE	83112 FineGb	83132 FineGb	83133 FineGb	83041 CoarGb	83043 CoarGb	83044 CoarGb	83045 CoarGb	83049 CoarGb	83050 CoarGb	83051 CoarGb	83053 CoarGb	83090 CoarGb	83095 CoarGb	83098 CoarGb
Ni	79.	79.	79.	79.	157.	79.	79.	79.	79	157.	79.	157.	79.	79.
Cr	68.	205.	205.	137.	410.	137.	137.	205.	410.	753.	53.	410.	479.	205.

Lagrande/Yasinski

SAMPLE	83099 CoarGb	83106 CoarGb	83118 CoarGb	83113 CoarGb	83134 CoarGb
SiO2	51.07	48.21	50.57	49.88	49.53
TiO2	0.14	0.90	0.68	0.43	0.57
Al2O3	15.08	15.27	14.60	15.78	13.70
MgO	11.67	8.40	8.29	11.35	11.09
FeO	5.63	10.75	10.13	8.00	9.72
MnO	0.13	0.22	0.21	0.13	0.18
CaO	9.80	11.13	10.87	6.30	10.94
Na2O	2.47	1.89	1.32	4.02	1.66
K2O	1.27	0.98	0.60	0.49	0.99
P2O5	0.01	0.06	0.05	0.03	0.04
LOI	3.65	2.21	2.46	4.17	1.98
	100.92	100.00	99.78	100.58	100.40

Cation proportions based on 100 cations

Si	47.25	45.72	48.48	46.31	46.22
Ti	0.10	0.64	0.49	0.30	0.40
Al	16.44	17.07	16.50	17.27	15.07
Mg	16.09	11.87	11.85	15.71	15.43
Fe	4.36	8.53	8.12	6.21	7.58
Mn	0.10	0.18	0.17	0.10	0.14
Ca	9.71	11.31	11.17	6.27	10.94
Na	4.43	3.48	2.45	7.24	3.00
K	1.50	1.16	0.73	0.58	1.18
P	0.01	0.05	0.04	0.02	0.03
O	152.62	152.65	155.69	151.37	152.12

Mg No.	0.787	0.582	0.593	0.717	0.670
Al/Al+Si	0.258	0.272	0.254	0.272	0.246

Geology of the Menarik Lake ultramafic complex

LEGEND

PROTEROZOIC

Diabase dykes

ARCHEAN

Serpentinites

Metagabbros, associated dykes

Mafic and intermediate tuffs

Quartzites, greywackes

Granodiorites, tonalites

Massive granites

Conglomerates

SYMBOLS

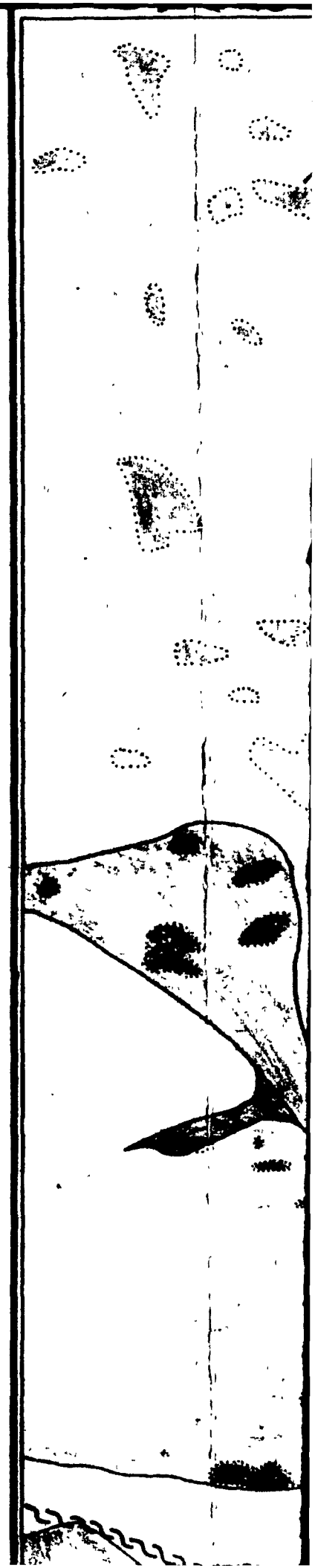

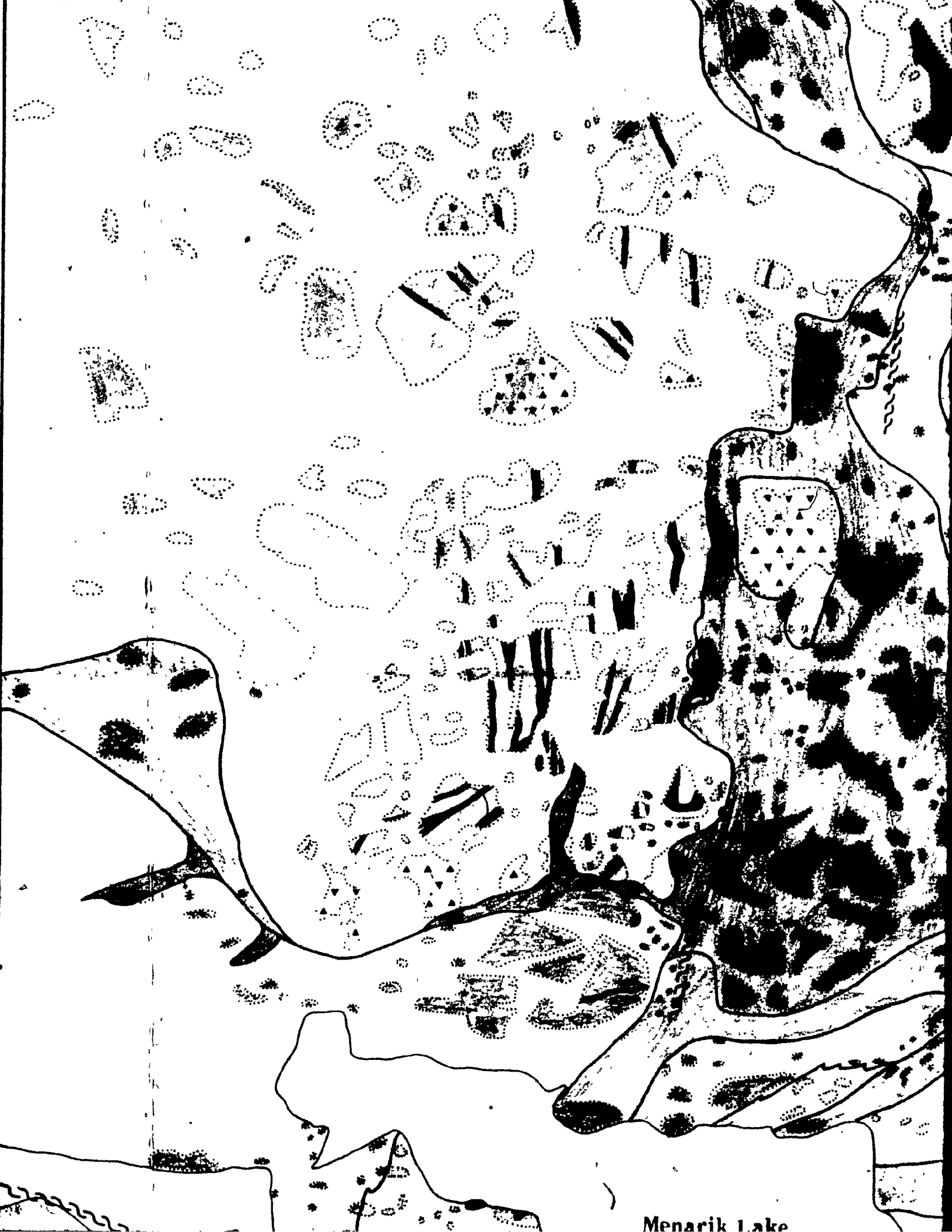
Menarik Lake

lenarik Lake

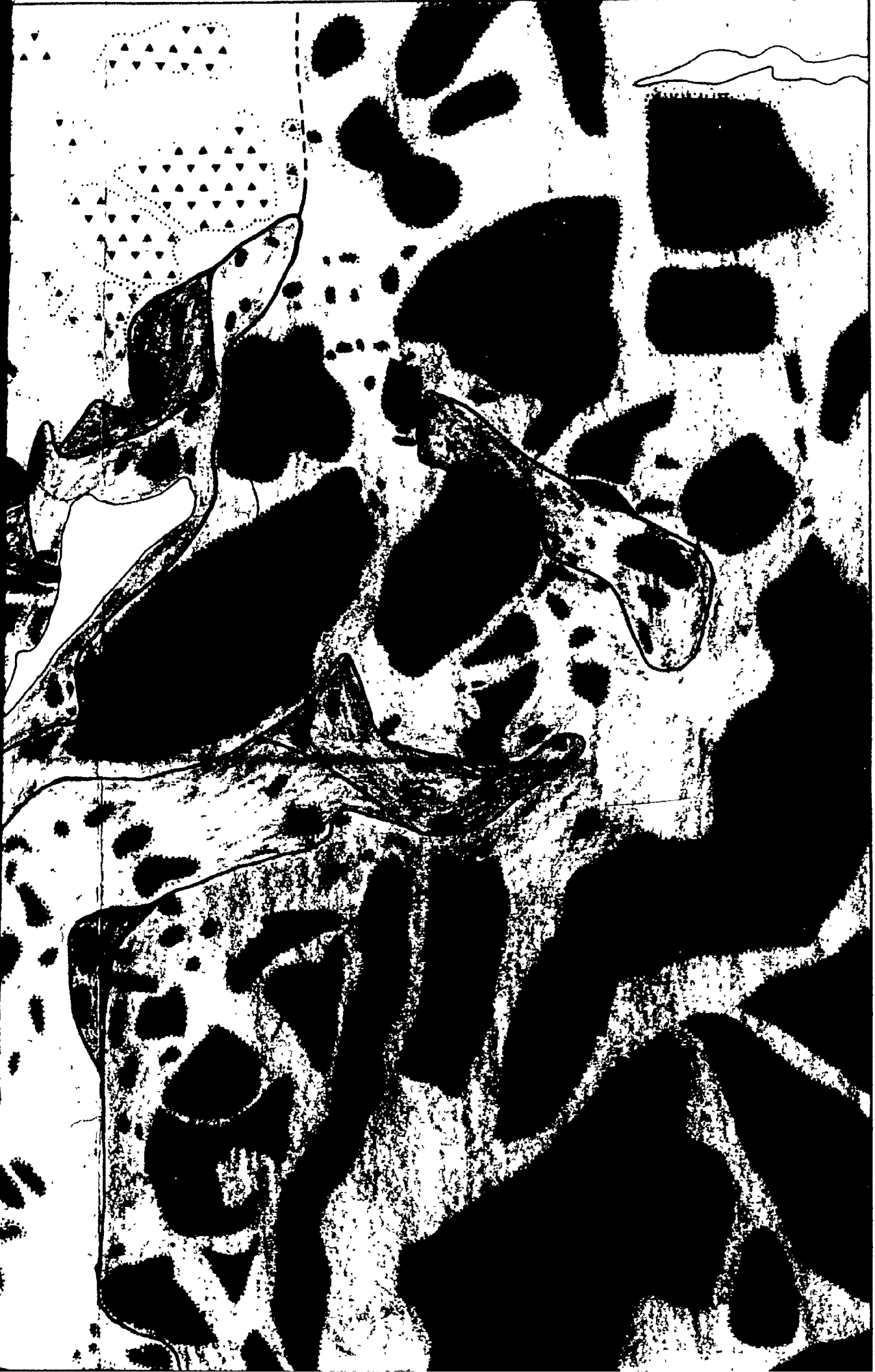

Massive granites

Conglomerates

SYMBOLS

Area of outcrop

Geological boundary (defined, approximate)

Fault

Bedding

Foliation

Axis of minor folds

Synform

Antiform

Metagabbro dykes not mapped in detail

Geological interpretation: Benoit Rivard, 1984

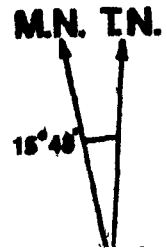

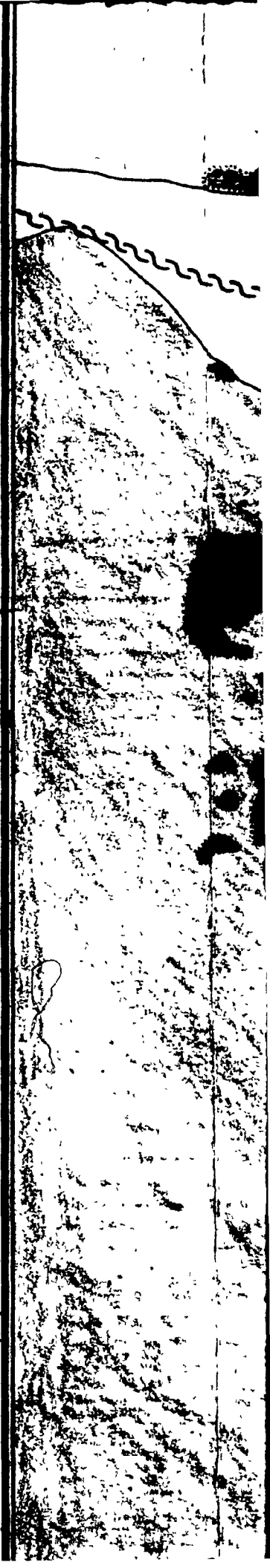

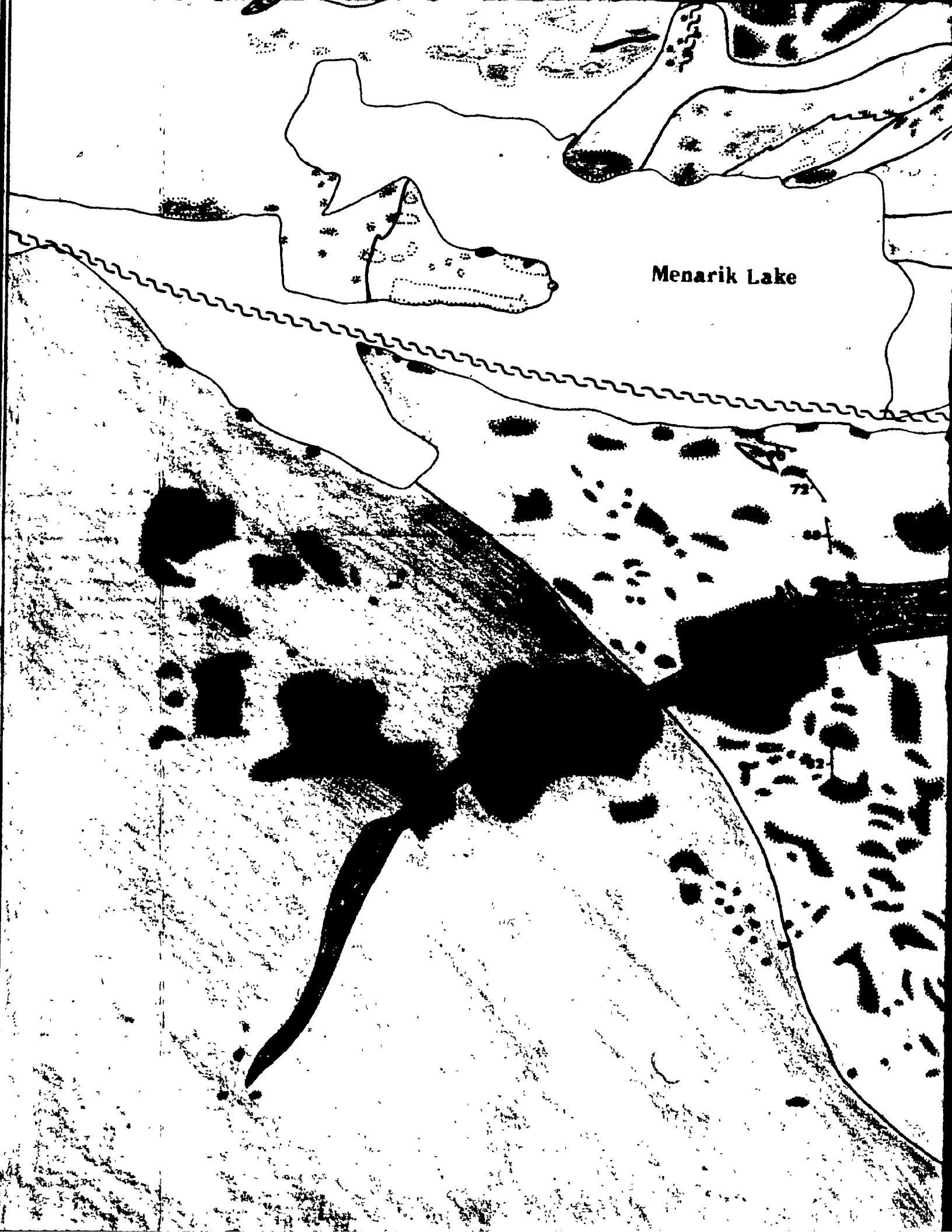
Menarik Lake


Menarik Lake
72
88
82
80
81


Lake
75
72


50
28
85
75
70

Metagabbro dykes not mapped in detail

Geological interpretation: Benoit Rivard, 1984

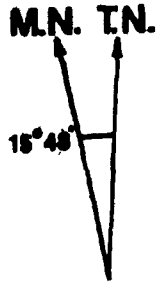

Scale 1:5000

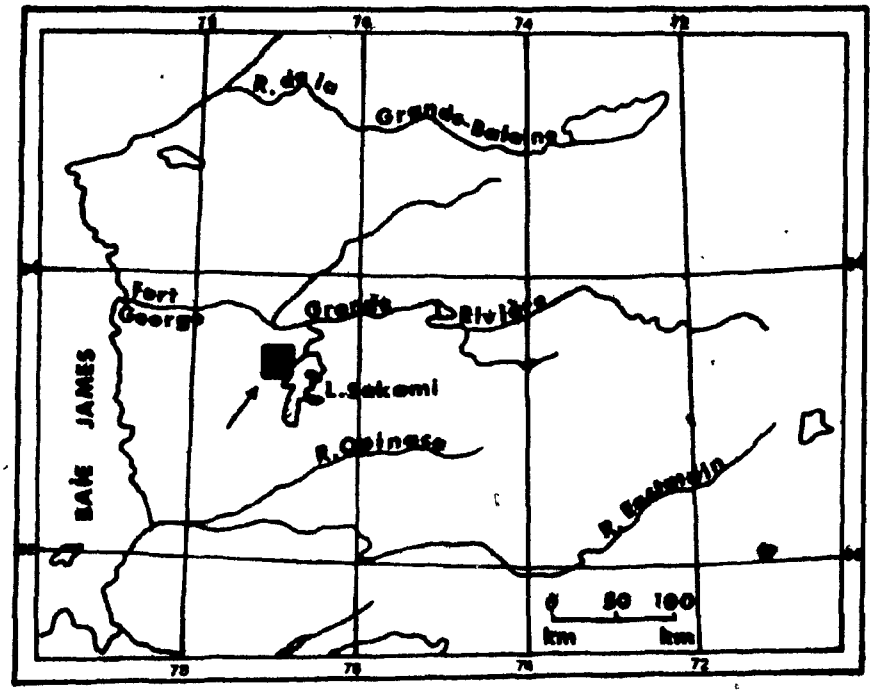

53°22'30"

77°20'12"

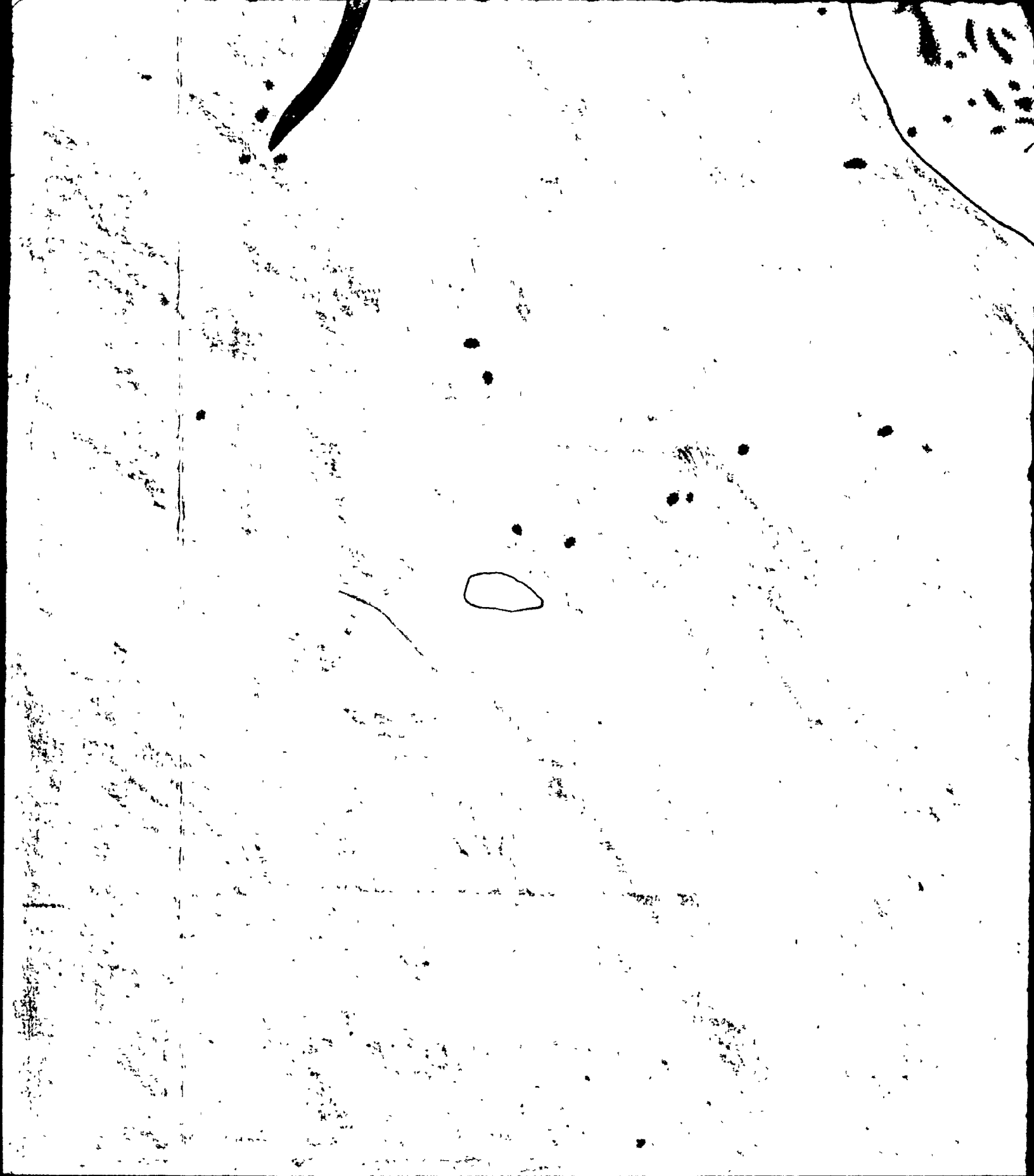

'12"


81
84
85
83

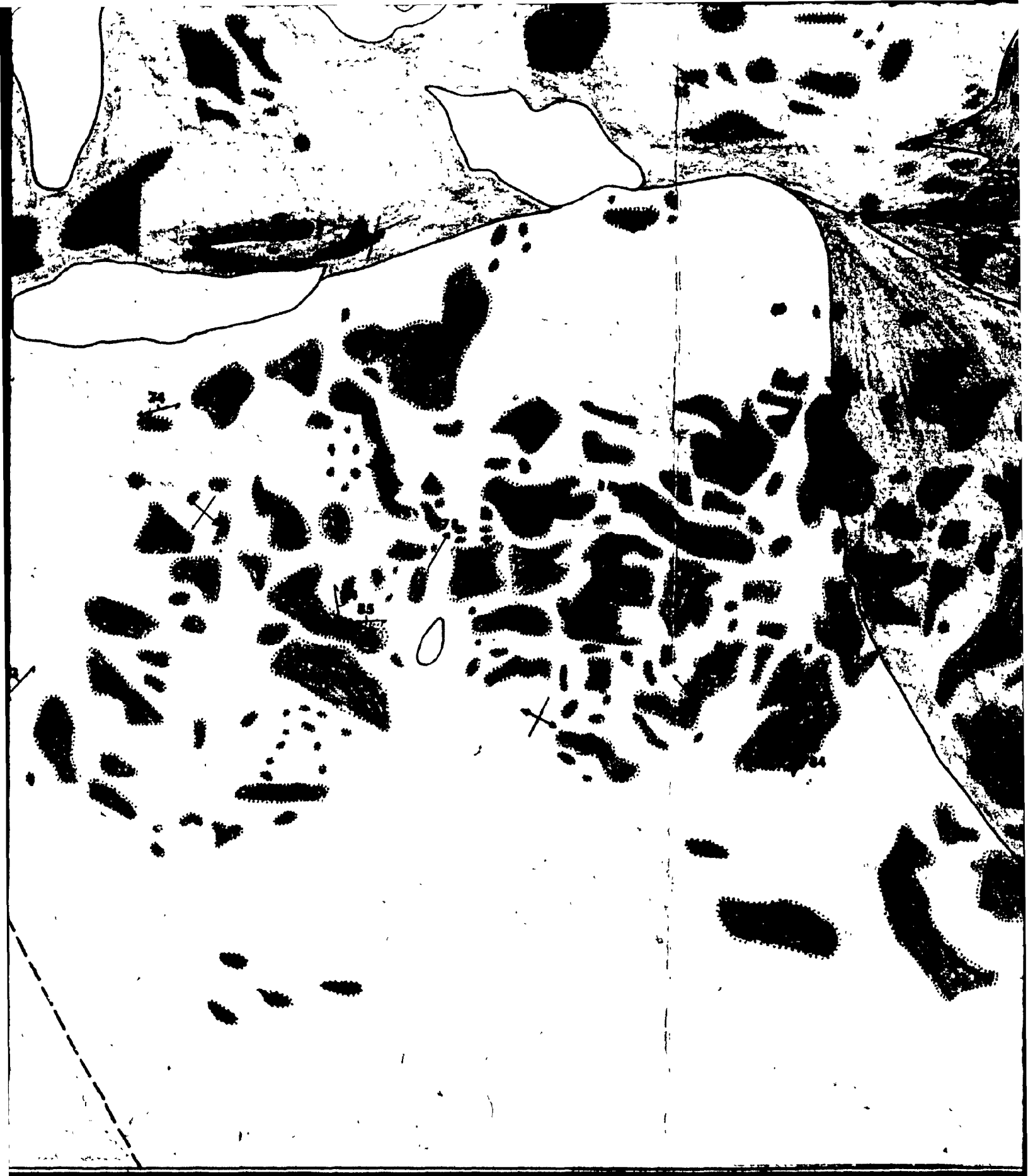


53°22'30"
77°17'00"